Annu. Rev. Nucl. Part. Sci. 1999. 49:303–39
Copyright © 1999 by Annual Reviews. All rights reserved

SPIN STRUCTURE FUNCTIONS

E. W. Hughes
California Institute of Technology, Pasadena, California 91125;
e-mail: Emlyn@slac.stanford.edu

R. Voss
CERN, CH-1211 Geneva 23, Switzerland; e-mail: Rudiger.Voss@cern.ch

Annu. Rev. Nucl. Part. Sci. 1999.49:303-339. Downloaded from arjournals.annualreviews.org
by MASSACHUSETTS INSTITUTE OF TECHNOLOGY on 05/05/08. For personal use only.

Key Words proton spin, deep inelastic scattering, quark-parton model, sum rules, quantum chromodynamics

■ **Abstract** We review the study of the internal spin structure of the proton and neutron. High-energy scattering of polarized leptons by polarized protons, neutrons, and deuterons provides a measurement of the nucleon spin structure functions. These structure functions give information on the polarized quark contributions to the spin of the proton and the neutron and allow tests of the quark-parton model and quantum chromodynamics. We discuss the formalism of deep inelastic scattering of polarized leptons on polarized nucleons, the past decade of experimental progress, and future programs to measure the polarized gluon contribution to the proton spin.

CONTENTS

0163-8998/99/1201-0303$08.00

Annu. Rev. Nucl. Part. Sci. 1999.49:303-339. Downloaded from arjournals.annualreviews.org
by MASSACHUSETTS INSTITUTE OF TECHNOLOGY on 05/05/08. For personal use only.

1. INTRODUCTION

1.1 Deep Inelastic Lepton-Nucleon Scattering

For 40 years now, high-energy lepton-nucleon scattering has served as a sensitive probe for the substructure of the proton and neutron. Experiments with high-energy electrons, muons, and neutrinos have been used to characterize the parton substructure of the nucleon and to establish the current theory of the strong interaction, quantum chromodynamics (QCD). Leptons provide a wonderfully clean probe of the nucleon's substructure, since they only interact with quarks via the electromagnetic interaction and are transparent to strong interactions within the nucleon. Among the accomplishments of this field of physics are the observation of scaling violation for the unpolarized nucleon structure functions, the measurement of the strong coupling constant $\alpha_s(Q^2)$, the confirmation of numerous QCD sum rules, and the extraction of the parton and gluon distributions inside the nucleon. Electron–proton scattering at collider energies ($\sim$300 GeV in the center of mass) has allowed the study of nucleon structure over an enormous kinematic range.

Trailing close behind the unpolarized deep inelastic scattering (DIS) experiments has been a polarized DIS program aimed at studying the spin structure of the nucleon using polarized lepton beams (electrons and muons) scattered by polarized targets. These fixed-target experiments have been used to characterize the spin structure of the proton and neutron and to test additional fundamental QCD and quark-parton model (QPM) sum rules. The first experiments in polarized electron–polarized proton scattering, performed in the 1970s, helped establish the parton structure of the proton. In the late 1980s, a polarized muon–polarized proton experiment found that a QPM sum rule was violated, which seemed to indicate that the quarks do not account for the spin of the proton. This "proton-spin crisis" gave birth to a new generation of experiments at several high-energy physics laboratories around the world. The new and extensive data sample collected from these fixed-

target experiments has enabled a careful characterization of the spin-dependent parton substructure of the nucleon. The results have been used to test QCD, to find an independent value for $\alpha_s(Q^2)$, to probe with reasonable precision the polarized parton distributions, and to provide a first look at the polarized gluon distribution.

Results from the experiments discussed in this chapter indicate that the quark contribution to the proton's and neutron's spin is approximately one third, and the results appear to indicate that the gluon contribution to the nucleon spin may be large. Future experiments at higher energies will focus on the polarized gluon contribution to the proton spin.

Annu. Rev. Nucl. Part. Sci. 1999.49:303-339. Downloaded from arjournals.annualreviews.org
by MASSACHUSETTS INSTITUTE OF TECHNOLOGY on 05/05/08. For personal use only.

1.2 The Spin of the Proton and Neutron

In quantum mechanics, the spin of the proton, neutron, and electron is equal to Planck's constant divided by two, $\frac{\hbar}{2}$. The convention is to drop the units of $\hbar$ (i.e. Joules-seconds) when discussing the nucleon spin structure. As far as we can tell today, the electron has no substructure, but the proton and neutron each have a complicated internal structure.

The primary motivation behind polarized DIS experiments is to establish the relationship between the simple spin $1/2$ of the nucleon to its internal structure, consisting of quarks and gluons. The following relation represents the decomposition of the proton spin:

$$\text{proton spin} = \frac{1}{2} = \Delta q + L_q + \Delta G + L_G, \qquad 1.$$

where Δq is the intrinsic quark contribution to the proton spin, ΔG is the gluon contribution, and L_q and L_G are the quark and gluon angular momentum contributions, respectively. The separation of the quark and gluon contributions into these pieces is not actually a gauge-invariant process (1). However, within some well-defined renormalization and factorization schemes, the contributions from the quarks and gluons can be determined.

The main impact of the experiments we describe has been their ability to uncover the contributions of quarks (Δq) to the proton spin. Some information on ΔG also is gleaned from the perturbative QCD analysis discussed in Section 5.

A primary assumption in all studies is that isospin symmetry is valid. This assumption implies that the only difference between a proton and a neutron is that a proton has an up quark, which is equivalent to a down quark in the neutron. If this is true, then the total quark contribution is the same for a proton and a neutron.

2. POLARIZED DEEP INELASTIC LEPTON SCATTERING

2.1 Kinematics, Cross Sections, and Asymmetries

The lowest order diagram for deep inelastic lepton scattering,

$$\ell + N \rightarrow \ell + X, \qquad 2.$$

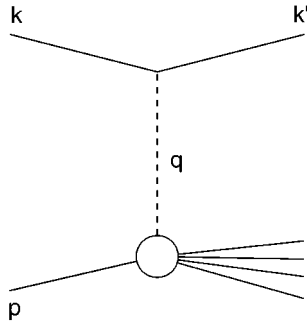

Figure 1 The lowest order Feynman diagram for deep inelastic lepton scattering.

Annu. Rev. Nucl. Part. Sci. 1999.49:303-339. Downloaded from arjournals.annualreviews.org
by MASSACHUSETTS INSTITUTE OF TECHNOLOGY on 05/05/08. For personal use only.

is shown in Figure 1. For neutral-current reactions of charged leptons, the interaction can be mediated by a virtual photon or a Z boson. At present fixed-target energies, the cross section for scattering of charged leptons is dominated by virtual photon exchange, and we neglect here the Z-exchange contribution.

In this chapter, we focus on inclusive scattering where the scattering amplitudes are summed over all possible hadronic final states. The unpolarized inclusive cross section can be written as a function of two independent kinematic variables. It is customary to choose two of the following Lorentz-invariant variables:

1. The squared four-momentum transfer,

$$Q^2 = -q^2 = -(k - k')^2 = 4EE' \sin^2 \theta; \qquad 3.$$

2. the energy transfer to the hadronic system,

$$\nu = p \cdot q/M = E' - E; \qquad 4.$$

3. the Bjorken scaling variable,

$$x = Q^2/2p \cdot q = Q^2/2M\nu; \qquad 5.$$

4. the scaling variable,

$$y = p \cdot q/p \cdot k = \nu/E. \qquad 6.$$

In these equations, k, k', p, and q are the four-vectors of the initial- and final-state lepton, the target nucleon, and the exchanged boson. M is the mass of the target nucleon, whereas the lepton mass has been neglected. E, E', and θ are the energies of the incident and scattered lepton, and the lepton scattering angle, in the laboratory frame.

Neglecting lepton masses, the differential cross section for unpolarized deep inelastic charged lepton scattering can be written, in the Born approximation, as (e.g. 2)

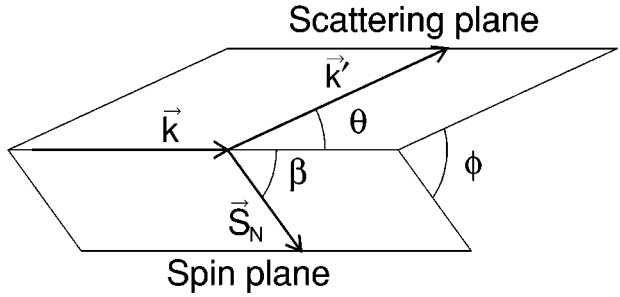

Figure 2 Scattering of longitudinally polarized leptons in the laboratory frame.

$$\frac{d^2\sigma}{dQ^2dx} = \frac{4\pi\alpha^2}{Q^4}\frac{1}{x}\left[xy^2F_1(x, Q^2) + \left(1 - y - \frac{Mxy}{2E}\right)F_2(x, Q^2)\right], \qquad 7.$$

where α is the electromagnetic coupling constant and $F_1(x, Q^2)$ and $F_2(x, Q^2)$ are the unpolarized structure functions of the nucleon. In the laboratory system, the polarized scattering process is conveniently visualized in the two planes depicted in Figure 2. The scattering plane is defined by the momentum three-vectors $\vec{k}$ and $\vec{k}'$ of the incoming and scattered lepton, respectively. The spin plane is defined by $\vec{k}$ and by the spin vector $\vec{S}_N$ of the nucleon; β is the angle between $\vec{k}$ and $\vec{S}_N$ ($0 \leq \beta \leq \pi$) and ϕ is the angle between the scattering and the spin planes.

The cross section for polarized scattering depends, in addition, on the relative orientation ϕ of the scattering and spin planes. This cross section can be decomposed into an unpolarized piece σ_0 and a polarized piece $\Delta\sigma$,

$$\frac{\mathrm{d}^3\sigma(\beta)}{\mathrm{d}Q^2\,\mathrm{d}x\,\mathrm{d}\phi} = \frac{\mathrm{d}^3\sigma_0}{\mathrm{d}Q^2\,\mathrm{d}x\,\mathrm{d}\phi} - \frac{\mathrm{d}^3\Delta\sigma(\beta)}{\mathrm{d}Q^2\,\mathrm{d}x\,\mathrm{d}\phi}, \qquad 8.$$

where $\mathrm{d}^3\sigma_0/\mathrm{d}x\,\mathrm{d}y\,\mathrm{d}\phi$ is the unpolarized cross section of Equation 7. In the Born approximation, the polarized contribution is (3)

$$\begin{aligned}\frac{\mathrm{d}^3\Delta\sigma(\beta)}{\mathrm{d}Q^2\,\mathrm{d}x\,\mathrm{d}\phi} = \frac{4\alpha^2}{Q^4}y\Bigg\{&\cos\beta\left[\left(1 - \frac{y}{2} - \frac{\gamma^2y^2}{4}\right)g_1(x, Q^2) - \frac{\gamma^2y}{4}g_2(x, Q^2)\right] \\ &- \cos\phi\sin\beta\frac{\sqrt{Q^2}}{\nu}\left(1 - y - \frac{\gamma^2y^2}{4}\right)^{\frac{1}{2}} \\ &\times\left[\frac{y}{2}g_1(x, Q^2) + g_2(x, Q^2)\right]\Bigg\}, \qquad 9.\end{aligned}$$

where

$$\gamma = \frac{2Mx}{\sqrt{Q^2}} \qquad 10.$$

and g_1, g_2 are the spin-dependent structure functions of the nucleon.

Annu. Rev. Nucl. Part. Sci. 1999.49:303-339. Downloaded from arjournals.annualreviews.org
by MASSACHUSETTS INSTITUTE OF TECHNOLOGY on 05/05/08. For personal use only.

Annu. Rev. Nucl. Part. Sci. 1999.49:303-339. Downloaded from arjournals.annualreviews.org
by MASSACHUSETTS INSTITUTE OF TECHNOLOGY on 05/05/08. For personal use only.

An inspection of Equation 9 reveals how the two structure functions g_1 and g_2 can be disentangled from measurements of the differential cross section. A target polarization parallel to the beam direction, i.e. $\sin\beta = 0$, mainly projects out g_1, since the contribution from g_2 is suppressed at high energies by the factor $Mx/2E$. For $\cos\beta = 0$, i.e. transverse target polarization, g_1 and g_2 contribute to the cross section with similar weights.

The polarized piece (Equation 9) gives a small contribution to the cross section and is, in general, experimentally suppressed by incomplete beam and target polarizations. It is therefore customary to evaluate it from measurements of cross-section asymmetries in which the unpolarized part in Equation 8 cancels. When both the beam and the target are longitudinally polarized ($\sin\beta = 0$), this asymmetry is

$$A_\parallel = \frac{\sigma^{\uparrow\downarrow} - \sigma^{\uparrow\uparrow}}{\sigma^{\uparrow\downarrow} + \sigma^{\uparrow\uparrow}}, \qquad 11.$$

where $\sigma^{\uparrow\downarrow}$ and $\sigma^{\uparrow\uparrow}$ are the cross sections for opposite and equal spin directions, respectively. For simplicity, terms of order γ^2 are neglected in the following discussion. From Equation 9,

$$A_\parallel = D[A_1 + \eta A_2], \qquad 12.$$

where

$$A_1(x) = \frac{g_1(x)}{F_1(x)}, \qquad 13.$$

and

$$A_2(x) = \gamma \frac{g_1(x) + g_2(x)}{F_1(x)}. \qquad 14.$$

D is often called the depolarization factor of the virtual photon and is given by

$$D = \frac{2y - y^2}{2(1-y)(1+R) + y^2}. \qquad 15.$$

The factor η depends only on kinematic variables:

$$\eta = \frac{\sqrt{Q^2}}{E} \frac{2(1-y)}{y(2-y)}. \qquad 16.$$

A_1 and A_2 can be interpreted as virtual photon-nucleon asymmetries. For spin-$\frac{1}{2}$ targets (proton and neutron),

$$A_1^{\mathrm{p,n}} = \frac{\sigma_{1/2} - \sigma_{3/2}}{\sigma_{1/2} + \sigma_{3/2}} \qquad 17.$$

and

$$A_2^{\mathrm{p,n}} = \frac{2\sigma^{TL}}{\sigma_{1/2} + \sigma_{3/2}}, \qquad 18.$$

whereas for the deuteron (4),

$$A_1^{\mathrm{d}} = \frac{\sigma_0 - \sigma_2}{\sigma_0 + \sigma_2} \qquad 19.$$

and

$$A_2^{\mathrm{d}} = \frac{\sigma_0^{TL} + \sigma_1^{TL}}{\sigma_0 + \sigma_2}. \qquad 20.$$

In these expressions, the indices refer to the total spin projections of the photon-hadron system in the direction of the virtual photon, and the σ^{TL} are cross sections arising from the interference of amplitudes for longitudinally and transversely polarized virtual photons. The following bounds can be derived for A_1 and A_2 (5):

$$|A_1| \leq 1, \qquad |A_2| \leq R. \qquad 21.$$

For this reason, A_2 is expected to give a small contribution to $A_\parallel$.

The transverse asymmetry $A_\perp$ is determined from the scattering of a longitudinally polarized beam on a transversely polarized target ($\sin\beta = 1$),

$$A_\perp = \frac{\sigma^{\downarrow\rightarrow} - \sigma^{\uparrow\rightarrow}}{\sigma^{\downarrow\rightarrow} + \sigma^{\uparrow\rightarrow}}, \qquad 22.$$

and is related to A_1 and A_2 by

$$A_\perp = d\left[A_2 - \gamma\left(1 - \frac{y}{2}\right)A_1\right], \qquad 23.$$

where

$$d = \frac{\sqrt{1-y}}{1-\frac{y}{2}}D. \qquad 24.$$

Finally, the experimentally measured counting-rate asymmetries A_{exp} are related to the cross-section asymmetries A by

$$A_{exp} = f_t P_t P_b A, \qquad 25.$$

where A represents either $A_\parallel$ or $A_\perp$. In this expression, P_b is the beam polarization, P_t the polarization of the target nucleons, and f_t the target dilution factor, i.e. the fraction of polarized nucleons in the target material.

2.2 Structure Functions in the Naive Quark-Parton Model

The spin-independent structure functions F_1 and F_2 have a straightforward interpretation in the QPM:

$$F_1(x) = \frac{1}{2}\sum_i e_i^2[q_i(x) + \bar{q}_i(x)], \qquad 26.$$

Annu. Rev. Nucl. Part. Sci. 1999.49:303-339. Downloaded from arjournals.annualreviews.org
by MASSACHUSETTS INSTITUTE OF TECHNOLOGY on 05/05/08. For personal use only.

$$F_2(x) = \sum_i e_i^2 x[q_i(x) + \bar{q}_i(x)]. \quad 27.$$

They are thus related by the Callan-Gross relation, which holds true for spin-$\frac{1}{2}$ quarks:

$$F_2(x) = 2xF_1(x). \quad 28.$$

In these expressions, $q_i(x)$ and $\bar{q}_i(x)$ are the densities of quarks and antiquarks, respectively; i is the quark flavor and e_i the quark electric charges.

The interpretation of the spin-dependent structure function g_1 is equally simple,

$$g_1(x) = \frac{1}{2}\sum_i e_i^2 \Delta q_i(x), \quad 29.$$

where

$$\Delta q_i(x) = q_i^+(x) + \bar{q}_i^+(x) - q_i^-(x) - \bar{q}_i^-(x) \quad 30.$$

and where $q_i^+(x)$ ($q_i^-(x)$) is the density of quarks of flavor i with helicity parallel (antiparallel) to the nucleon spin. This interpretation of $g_1(x)$ can be understood from the fact that a virtual photon with spin projection $+1$ can only be absorbed by a quark with spin projection $-1/2$, and vice versa.

The interpretation of the "transverse" spin structure function g_2 in the QPM is less obvious and has been the subject of much theoretical debate (3). Wandzura & Wilczek (6) have shown that in QCD it can be decomposed as

$$g_2(x, Q^2) = g_2^{WW}(x, Q^2) + \bar{g}_2(x, Q^2), \quad 31.$$

where the "trivial" piece g_2^{WW} is a leading twist contribution (in the jargon of QCD) and is completely determined by $g_1(x, Q^2)$, as follows:

$$g_2^{WW}(x, Q^2) = -g_1(x, Q^2) + \int_x^1 g_1(y, Q^2)\frac{\mathrm{d}y}{y}. \quad 32.$$

The term $\bar{g}_2(x, Q^2)$ is a twist-3 contribution that is best understood in an operator product expansion (OPE) analysis in QCD, where it is sensitive to a quark-gluon correlation function in the nucleon and thus contains unique new physics.

2.3 The Bjorken Sum Rule

No theoretical predictions exist for the x dependence of spin-dependent structure functions. This is similar to the situation in unpolarized scattering. Definite predictions do exist, however, for the first moments,

$$\Gamma_1 = \int_0^1 g_1(x)\,\mathrm{d}x, \quad 33.$$

Annu. Rev. Nucl. Part. Sci. 1999.49:303-339. Downloaded from arjournals.annualreviews.org
by MASSACHUSETTS INSTITUTE OF TECHNOLOGY on 05/05/08. For personal use only.

of spin-dependent structure functions. The most fundamental of these is the celebrated Bjorken sum rule (7),

$$\Gamma_1^p - \Gamma_1^n = \frac{1}{6}\left|\frac{g_A}{g_V}\right|, \qquad 34.$$

where g_A and g_V are the axial and vector weak coupling constants of neutron β-decay. In this form, the sum rule was derived by Bjorken from light cone current algebra and isospin invariance.

In QCD, moments of structure functions can be analyzed in the OPE (8, 9). In this framework, the sum rule (Equation 34) can be derived in the limit $Q^2 \to \infty$. At finite values of Q^2, it is subject to radiative corrections (8, 10),

$$\Gamma_1^p(Q^2) - \Gamma_1^n(Q^2) = \frac{1}{6}\left|\frac{g_A}{g_V}\right|\left[1 - \frac{\alpha_s(Q^2)}{\pi} - \cdots\right], \qquad 35.$$

where α_s is the strong coupling constant. The QCD corrections have recently been computed up to $O(\alpha_s^3)$ (11) and the $O(\alpha_s^4)$ correction has also been estimated (12).

2.4 Quark-Parton Model Sum Rules

Separate sum rules for the proton and the neutron were derived by Ellis & Jaffe (13) for the proton and the neutron. Straightforward integration of Equation 29 gives, for three quark flavors,

$$\Gamma_1^p = \frac{1}{2}\left(\frac{4}{9}\Delta u + \frac{1}{9}\Delta d + \frac{1}{9}\Delta s\right), \qquad 36.$$

and, from isospin invariance,

$$\Gamma_1^n = \frac{1}{2}\left(\frac{1}{9}\Delta u + \frac{4}{9}\Delta d + \frac{1}{9}\Delta s\right), \qquad 37.$$

where

$$\Delta q_i = \int_0^1 [q^+(x) - q^-(x)]\,dx \qquad 38.$$

are the moments of spin-dependent parton distributions in the proton.[1] In the QPM, linear combinations of these moments are related to the weak axial-vector couplings a_0, a_3 and a_8 by (13)

$$a_0 = \Delta u + \Delta d + \Delta s \equiv \Delta\Sigma, \qquad 39.$$

$$a_3 = \Delta u - \Delta d = \left|\frac{g_A}{g_V}\right|, \qquad 40.$$

[1]The moments Δq_i must not be confused with the spin-dependent parton distributions $\Delta q_i(x)$ defined in Equation 30. Nevertheless, this notation has become widely used.

Annu. Rev. Nucl. Part. Sci. 1999.49:303-339. Downloaded from arjournals.annualreviews.org
by MASSACHUSETTS INSTITUTE OF TECHNOLOGY on 05/05/08. For personal use only.

$$a_8 = \Delta u + \Delta d - 2\Delta s, \qquad 41.$$

where Equation 40 is the Bjorken sum rule (Equation 34). The moments Δq_i can be interpreted as contribution of quark flavor q_i to the spin of the proton; $a_0 = \Delta\Sigma$ is thus the total quark contribution to the proton spin.

Equations 36 and 37 can now be cast into the form

$$\Gamma_1^{p(n)} = \frac{1}{12}\left[+ (-)a_3 + \frac{1}{3}a_8 \right] + \frac{1}{9}a_0. \qquad 42.$$

In flavor-SU(3) symmetry, a_3 and a_8 are related to the symmetric and antisymmetric weak $SU(3)_f$ couplings F and D of the baryon octet:

$$a_3 = \left| \frac{g_A}{g_V} \right| = F + D, \qquad 43.$$

$$a_8 = 3F - D. \qquad 44.$$

Provided that $SU(3)_f$ is an exact symmetry, measurements of F/D in hyperon decays can be used to numerically predict a_8. There is no theoretical prediction for the singlet axial coupling a_0. However, under the assumption that the strange sea in the nucleon is unpolarized (i.e. $\Delta s = 0$), $a_0 = a_8$ and Equation 42 takes the form

$$\Gamma_1^{p(n)} = +(-)\frac{1}{12}(F + D) + \frac{5}{36}(3F - D). \qquad 45.$$

These are the Ellis-Jaffe sum rules (13).

Equations 42 and 45 are valid in the scaling limit. Like the Bjorken sum rule, they can be derived in the OPE and are also subject to QCD radiative corrections at finite Q^2. The QCD correction to the flavor-nonsinglet term $\pm a_3 + a_8/3$ can be expressed as a coefficient function that is identical to the correction term to the Bjorken sum rule in Equation 35. The corresponding coefficient function for the singlet term a_0 has been computed up to order $O(\alpha_s^2)$ (9), and the $O(\alpha_s^3)$ term has been estimated (14). The QCD radiative corrections are sizable in the Q^2 range of the present experiments and are essential for the comparison and the correct interpretation of data taken at different Q^2 (15).

Nonperturbative higher twist effects are also expected to contribute to the Q^2 evolution of the moments of g_1 (16–23). These corrections have been the subject of considerable theoretical debate, and a source of some confusion, in the recent past. The consensus now seems to be that they are small in the kinematic range of the present data, and they have been neglected in most analyses.

Annu. Rev. Nucl. Part. Sci. 1999.49:303-339. Downloaded from arjournals.annualreviews.org
by MASSACHUSETTS INSTITUTE OF TECHNOLOGY on 05/05/08. For personal use only.

Annu. Rev. Nucl. Part. Sci. 1999.49:303-339. Downloaded from arjournals.annualreviews.org
by MASSACHUSETTS INSTITUTE OF TECHNOLOGY on 05/05/08. For personal use only.

2.5 Spin Structure Functions in Perturbative Quantum Chromodynamics

The treatment of g_1 in perturbative QCD follows closely that of unpolarized parton distributions and structure functions (24). The flavor-singlet (S) and nonsinglet (NS) combinations of the polarized quark and antiquark distributions are

$$\Delta\Sigma(x,t) = \sum_{i=1}^{n_f} \Delta q_i(x,t), \qquad 46.$$

$$\Delta q_{\rm NS}(x,t) = \frac{\sum_{i=1}^{n_f}\left(e_i^2 - \frac{1}{n_f}\sum_{k=1}^{n_f} e_k^2\right)}{\frac{1}{n_f}\sum_{k=1}^{n_f} e_k^2}\Delta q_i(x,t), \qquad 47.$$

where $t = \ln(Q^2/\Lambda^2)$, Λ is the scale parameter of QCD, and n_f is the number of active flavors. In this notation, g_1 is related to the polarized quark distributions and to the polarized gluon distribution $\Delta G(x,t)$ by coefficient functions C_q and C_g through

$$g_1(x,t) = \frac{1}{2}\sum_{k=1}^{n_f}\frac{e_k^2}{n_f}\int_x^1 \frac{{\rm d}y}{y}\left[C_q^{\rm S}\left(\frac{x}{y},\alpha_s(t)\right)\Delta\Sigma(y,t) + 2n_f C_g\left(\frac{x}{y},\alpha_s(t)\right)\Delta G(y,t) + C_q^{\rm NS}\left(\frac{x}{y},\alpha_s(t)\right)\Delta q_{\rm NS}(y,t)\right]. \qquad 48.$$

The t dependence of both unpolarized and polarized quark and gluon distributions follows the Dokshitzer-Gribov-Lipatov-Altarelli-Parisi (DGLAP) equations (25–27). The singlet and gluon distributions are coupled by

$$\frac{\rm d}{{\rm d}t}\Delta\Sigma(x,t) = \frac{\alpha_s(t)}{2\pi}\int_x^1 \frac{{\rm d}y}{y}\left[P_{qq}^{\rm S}\left(\frac{x}{y},\alpha_s(t)\right)\Delta\Sigma(y,t) + 2n_f P_{qg}\left(\frac{x}{y},\alpha_s(t)\right)\Delta G(y,t)\right], \qquad 49.$$

$$\frac{\rm d}{{\rm d}t}\Delta G(x,t) = \frac{\alpha_s(t)}{2\pi}\int_x^1 \frac{{\rm d}y}{y}\left[P_{gq}\left(\frac{x}{y},\alpha_s(t)\right)\Delta\Sigma(y,t) + P_{gg}\left(\frac{x}{y},\alpha_s(t)\right)\Delta G(y,t)\right], \qquad 50.$$

whereas the evolution of the nonsinglet distribution is independent of the singlet and gluon distributions:

$$\frac{\rm d}{{\rm d}t}\Delta q_{\rm NS}(x,t) = \frac{\alpha_s(t)}{2\pi}\int_x^1 \frac{{\rm d}y}{y} P_{qq}^{\rm NS}\left(\frac{x}{y},\alpha_s(t)\right)\Delta q_{\rm NS}(y,t). \qquad 51.$$

Annu. Rev. Nucl. Part. Sci. 1999.49:303-339. Downloaded from arjournals.annualreviews.org
by MASSACHUSETTS INSTITUTE OF TECHNOLOGY on 05/05/08. For personal use only.

The QCD splitting functions P_{gq} and P_{gg} are different for polarized and unpolarized parton distributions because of a soft gluon singularity at $x = 0$, which is only present in the unpolarized case. The ratio g_1/F_1 is therefore Q^2 dependent; however, in kinematic regions dominated by valence quarks, this Q^2 dependence is expected to be small (28).

Equations 48–51 are valid for all orders of perturbative QCD. The quark and gluon distributions, coefficient functions, and splitting functions depend on the mass factorization scale and on the renormalization scale; we adopt here the simplest choice, setting both scales equal to Q^2. At leading order, the coefficient functions are $C_q^{0,\mathrm{S}}(\frac{x}{y}, \alpha_s) = C_q^{0,\mathrm{NS}}(\frac{x}{y}, \alpha_s) = \delta(1 - \frac{x}{y})$ and $C_g^0(\frac{x}{y}, \alpha_s) = 0$, and g_1 decouples from ΔG.

Beyond leading order, the coefficient functions and splitting functions are not uniquely defined but depend on the renormalization and factorization scheme. Two schemes are commonly used in the analysis of polarized parton distributions, the modified minimal subtraction ($\overline{\mathrm{MS}}$) scheme (29) and the Adler-Bardeen (AB) (30) scheme. In the $\overline{\mathrm{MS}}$ scheme, the first moment of the gluon coefficient function vanishes and the gluon density $\Delta G(x, Q^2)$ does not contribute to $\Gamma_1 = \int_0^1 g_1(x)\,dx$. In the AB scheme, a term $\propto \alpha_s(Q^2)\Delta G(Q^2)$, which is attributable to the anomalous nonconservation of the singlet axial current (31), contributes explicitly to Γ_1. The first moments of the singlet quark distribution in the two schemes are related by

$$\Delta\Sigma_{\overline{\mathrm{MS}}}(Q^2) = \Delta\Sigma_{\mathrm{AB}} - n_f \frac{\alpha_s(Q^2)}{2\pi}\Delta G(Q^2). \qquad 52.$$

$\Delta\Sigma_{\mathrm{AB}}$ is independent of Q^2 even beyond leading order. At leading order, $\Delta G(Q^2)$ behaves as $1/\alpha_s$; therefore, this scheme dependence does not vanish at large Q^2.

The complete set of next-to-leading-order (NLO) coefficient functions and splitting functions in the $\overline{\mathrm{MS}}$ renormalization scheme can be found elsewhere (32, 33). This formalism allows for a complete NLO QCD analysis of spin-dependent structure functions.

3. POLARIZED LEPTON SCATTERING EXPERIMENTS

Table 1 provides an overview of polarized deep inelastic lepton-nucleon scattering experiments. All of these experiments are based on the principle of measuring cross-section asymmetries for the scattering of longitudinally polarized charged lepton beams on longitudinally or transversely polarized targets. They were pioneered by SLAC experiments E80 and E130 (Section 3.1), which used an electron beam with energies between 6 GeV and 23 GeV and a polarized butanol target. These two experiments provided the first measurements of the asymmetry A_1 and the structure function g_1 of the proton. However, their limited kinematic range precluded a meaningful test of sum rule predictions. The European Muon Collaboration (EMC) experiment at CERN (Section 3.3) repeated the SLAC measurements with a muon beam of ten times higher energy and a polarized ammonia

Annu. Rev. Nucl. Part. Sci. 1999.49:303-339. Downloaded from arjournals.annualreviews.org
by MASSACHUSETTS INSTITUTE OF TECHNOLOGY on 05/05/08. For personal use only.

TABLE 1 Experiments on polarized deep inelastic lepton-nucleon scattering

Experiment	Beam	Year[a]	Beam energy (GeV)	Target	References[b]
E80	e^-	1974–1976	6–19	C_4H_9OH	(34)
E130	e^-	1979–1980	16.2–22.7	C_4H_9OH	(35)
EMC	μ^+	1984–1985	100–200	NH_3	(36)
SMC	μ^+	1992	100	C_4D_9OD	(37)
		1993	190	C_4H_9OH	(38, 39, 40)
		1994	190	C_4D_9OD	(41)
		1995	190	C_4D_9OD	(42)
		1996	190	NH_3	(43)
		1992–1996	100–190		(44)
E142	e^-	1992	19.4–25.5	^3He	(45, 46)
E143	e^-	1993	29.1	NH_3, ND_3	(47–51)
E154	e^-	1995	50	^3He	(52, 53)
E155	e^-	1996	50	NH_3, ND_3	
HERMES	e^-	1995–	30–35	H, D, ^3He	(54, 55)

[a]Period of data taking.

[b]References to the principal results on asymmetries and structure functions obtained to date.

target. EMC discovered the violation of the Ellis-Jaffe sum rule for the proton. Starting in the early 1990s, a new generation of high-precision experiments was set up at SLAC (Section 3.2), CERN (Section 3.4), and DESY (Section 3.5). These experiments have made the first measurements with polarized neutron and deuteron targets, testing the Bjorken sum rule and QCD predictions for the Q^2 evolution of spin-dependent structure functions.

3.1 Early SLAC Experiments

The first experiments involving the scattering of a polarized electron beam off a polarized target were performed at SLAC. These early experiments came relatively soon after the discovery of the partonic substructure of the proton and were geared toward testing the QPM (56). If the proton is made up of free quarks, two up and one down, then the wave function [called the SU(6) wave function (57)] can be written as

$$|p^\uparrow\rangle = \frac{1}{\sqrt{18}}[2|u^\uparrow u^\uparrow d^\downarrow\rangle + 2|u^\uparrow d^\downarrow u^\uparrow\rangle + 2|d^\downarrow u^\uparrow u^\uparrow\rangle - |u^\uparrow u^\downarrow d^\uparrow\rangle - |u^\uparrow d^\uparrow u^\downarrow\rangle - |d^\uparrow u^\uparrow u^\downarrow\rangle - |u^\downarrow u^\uparrow d^\uparrow\rangle - |u^\downarrow d^\uparrow u^\uparrow\rangle - |d^\uparrow u^\downarrow u^\uparrow\rangle]. \quad 53.$$

To obtain the probability P of an up or down quark with its spin parallel ($\uparrow$) or antiparallel ($\downarrow$) to the nucleon spin, one simply squares the wave function:

$$P(u^{\uparrow}) = 5/9 \qquad P(u^{\downarrow}) = 1/9$$
$$P(d^{\uparrow}) = 1/9 \qquad P(d^{\downarrow}) = 2/9.$$

The value of the asymmetry A_1 for the proton is given by the square of the charges of each quark flavor and the probability that the quark is found parallel versus antiparallel to the nucleon spin, namely

$$A_1^p = \frac{4/9[P(u^{\uparrow}) - P(u^{\downarrow})] + 1/9[P(d^{\uparrow}) - P(d^{\downarrow})]}{4/9[P(u^{\uparrow}) + P(u^{\downarrow})] + 1/9[P(d^{\uparrow}) + P(d^{\downarrow})]}.$$

The proton asymmetry becomes $A_1^p = 5/9$ and the neutron asymmetry is found by interchanging the up-quark and down-quark probabilities, yielding $A_1^n = 0$.

As mentioned above, the first two SLAC experiments, E80 (34) and E130 (35), scattered polarized electrons with energies between 10 GeV and 23 GeV off polarized butanol targets. The protons in the butanol targets contributed to the spin-dependent scattering, whereas the carbon and oxygen nuclei, having spin 0, provided only a dilution to the measured asymmetry. At these relatively high energies, the four-momentum transfer of the interaction Q^2 was greater than 1 GeV^2, and the process is considered to be in the deep inelastic scattering regime.

The two SLAC experiments were truly pioneering in that many different experimental techniques had to be pulled together to perform the measurement. For example, E80 was the first experiment to produce a polarized electron beam by stripping the electrons from a beam of polarized lithium atoms. In addition, E80 and E130 were the first to study the depolarization of solid targets in a relatively high-current electron beam. The experimental techniques developed in these early experiments have led to an entire class of parity-violation electron scattering experiments to study the electroweak theory (58, 59) as well as ultimately establishing the modern-day deep inelastic scattering programs discussed later in this section.

The results from SLAC experiments E80 and E130 confirmed the early QPM prediction that the proton asymmetries would be large and positive. Figure 3 presents the results from these early experiments compared with the prediction from the SU(6) model. Although SU(6) is known to break down because of the existence of sea quarks and gluons, it appears to work well experimentally at $x \simeq 0.3$.

There is some evidence for an x dependence in the measured asymmetries. In particular, the smaller values of A_1 at small x compared with the theory eventually provoked a decade-long pursuit to test in detail the spin structure of the proton and neutron as it relates to QPM and QCD predictions. The first look at higher-energy muon scattering, discussed in the next section, rapidly advanced our knowledge of the proton spin structure.

Annu. Rev. Nucl. Part. Sci. 1999.49:303-339. Downloaded from arjournals.annualreviews.org
by MASSACHUSETTS INSTITUTE OF TECHNOLOGY on 05/05/08. For personal use only.

Annu. Rev. Nucl. Part. Sci. 1999.49:303-339. Downloaded from arjournals.annualreviews.org
by MASSACHUSETTS INSTITUTE OF TECHNOLOGY on 05/05/08. For personal use only.

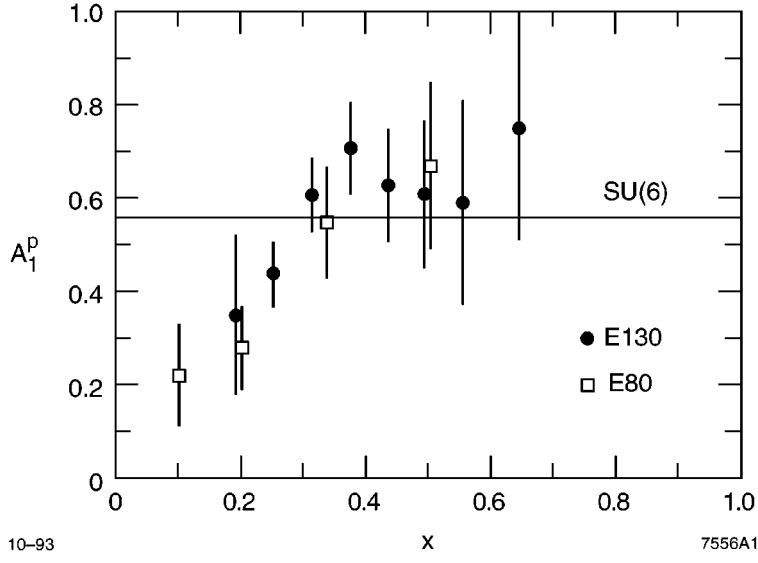

Figure 3 Proton asymmetry results A_1^p from SLAC experiments E80 and E130 compared with the SU(6) wave-function prediction $A_1^p = \frac{5}{9}$.

3.2 Recent SLAC Experiments

Over the past decade, in response to the proton-spin crisis created by the EMC experiment (36), the SLAC fixed-target program focused on deep inelastic scattering experiments to study the spin structure of the proton and neutron. The SLAC experiments scattered polarized electrons with energies ranging from 10 GeV to 50 GeV off polarized targets and detected the scattered electrons in spectrometer arms (see Figure 4), located at angles of 3–10 degrees. Within the spectrometer (46), a detector package consisting of Cerenkov counters, hodoscope tracking scintillators, and lead-glass calorimeters was used to identify the scattered electrons and determine their momenta.

A few experimental techniques are special to the SLAC experiments. The electron beam is produced in bunches at 120 Hz and the spin direction of the beam can be reversed randomly on a pulse-to-pulse basis, allowing an essentially simultaneous measurement of $\sigma^{\uparrow\uparrow}$ and $\sigma^{\downarrow\uparrow}$. In the past few years, the beam polarization has increased to near 80%, thanks to the development of new strained GaAs technology at the electron source (60).

The SLAC experiments have provided results on the proton, deuteron, and neutron spin structure functions, using polarized solid targets of ammonia for the proton studies, deuterated ammonia and lithium deuteride for the deuteron studies, and polarized helium-3 for the neutron studies. The polarized lithium contribution in a lithium deuteride target is modeled as being closely related to an unpolarized

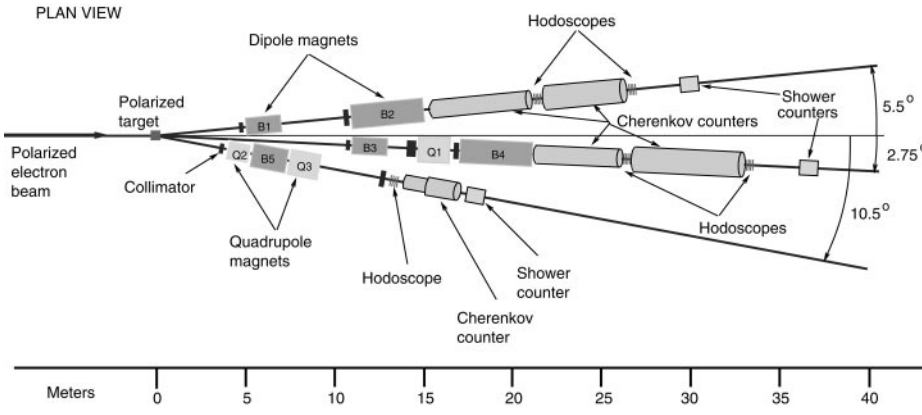

Figure 4 Schematic of spectrometers used in the SLAC polarized fixed-target program.

helium-4 nucleus bound to a polarized deuteron. The polarized helium-3 nucleus is modeled as a polarized neutron bound to two unpolarized protons whose spins are antiparallel to one another owing to the Pauli Exclusion Principle.

The series of experiments run at SLAC over the past decade collected data for one or two months each year and recorded approximately one scattered electron event per pulse. At this rate, the experiments each typically recorded 100–300 million events. When grouped into x bins, raw asymmetries were measured to a precision of typically 10^{-3}, resulting in statistical uncertainties of a few percent on the physics asymmetry A_1, corrected for beam and target polarizations and various dilutions. The high electron-beam current matched to the thick targets led to results with high statistical precision.

3.3 The EMC Experiment at CERN

The EMC experiment (36) was performed in the high-energy muon beam of the CERN SPS (61). This beam was produced from the decay of pions and kaons in flight. Because of parity violation in the weak decay $\pi(K) \rightarrow \mu\nu_\mu$, it had a natural longitudinal polarization, which depends on the ratio of muon and pion (kaon) energies (62). Because neither hadron nor muon beams were monochromatic but both have a finite phase space, the average beam polarization was evaluated by a Monte Carlo simulation. The muon/pion energy ratio was chosen to obtain an optimal combination of polarization and muon intensity; the beam polarizations in the CERN experiments were typically 80%. The beam momentum was measured with a magnetic spectrometer, which was integrated with the beam transport system.

The polarized target (63) was subdivided in two cells, each filled with about 1 liter of solid ammonia. The protons in the two cells were polarized in opposite directions in a strong magnetic field using the technique of dynamic nuclear polarization. This arrangement allowed the data with parallel and antiparallel orientation of muon and proton spin required to evaluate the longitudinal asymmetry

Annu. Rev. Nucl. Part. Sci. 1999.49:303-339. Downloaded from arjournals.annualreviews.org
by MASSACHUSETTS INSTITUTE OF TECHNOLOGY on 05/05/08. For personal use only.

Annu. Rev. Nucl. Part. Sci. 1999.49:303-339. Downloaded from arjournals.annualreviews.org
by MASSACHUSETTS INSTITUTE OF TECHNOLOGY on 05/05/08. For personal use only.

A (Equation 11) to be recorded simultaneously, thus eliminating time-dependent systematic errors in the measurement. To suppress further experimental uncertainties, the polarizations of both target cells were reversed in regular intervals. The proton polarization was measured with nuclear magnetic resonance techniques, and varied between 70% and 80%.

The scattered muons were measured with a large-aperture, high-resolution magnetic spectrometer (64), using large arrays of scintillation counters for triggering and different types of wire chambers for track reconstruction. The layout of this spectrometer is very similar to the one used by the Spin Muon Collaboration (SMC) experiment, which is discussed in more detail below.

3.4 The Spin Muon Collaboration Experiment at CERN

The SMC experimental setup was similar to that used by the EMC collaboration. It used the same beam as the EMC experiment; the beam optics were improved to provide a smaller beam spot at the target location. A beam polarimeter, downstream of the scattered-muon spectrometer, allowed measurement of the beam polarization either by muon scattering on polarized electrons in a magnetized foil (40, 66) or by measuring the Michel spectrum of positrons from μ^+ decay (40, 65).

The polarized target design (67) was based on the same principles as the EMC target, consisting of two 60-cm-long cylindric target cells separated by a 30-cm gap. Solid butanol and deuterated butanol, respectively, were used as target material for most of the data taking; solid ammonia was used for the last data-taking period in 1996. A dipole magnet allowed polarization of the target in a direction transverse to the beam so that the asymmetry A_2 could be measured. Typical target polarizations were close to 90% for the proton targets and about 50% for the deuteron targets.

The SMC spectrometer (Figure 5) is based on a conventional wide-aperture dipole magnet operated with a bending power of 4.4 Tm at a beam energy of 190 GeV. The scattered muons are measured in a large array of multiwire proportional chambers installed before, inside, and behind the magnet. The debris of hadrons produced in deep inelastic interactions is stopped in a 2-m-thick iron absorber. The scattered muons are identified by observing tracks in a second spectrometer stage, which consists of multiwire proportional chambers, streamer tubes, and drift tubes. The muon trigger is provided by predefined coincidence patterns between three arrays of plastic scintillation counters, two of which are installed behind the hadron absorber.

3.5 The HERMES Experiment at DESY

At DESY, an experiment named HERMES was built to scatter 27.5-GeV polarized electrons produced in a high-current storage ring off polarized gas targets and to detect the outgoing scattered particles in a large, open acceptance forward spectrometer (68). The electrons in the storage ring are polarized transversely to the beam direction via the Sokolov-Ternov effect (69), and the spins are rotated to the longitudinal direction using spin rotators. The polarized gas targets consist of

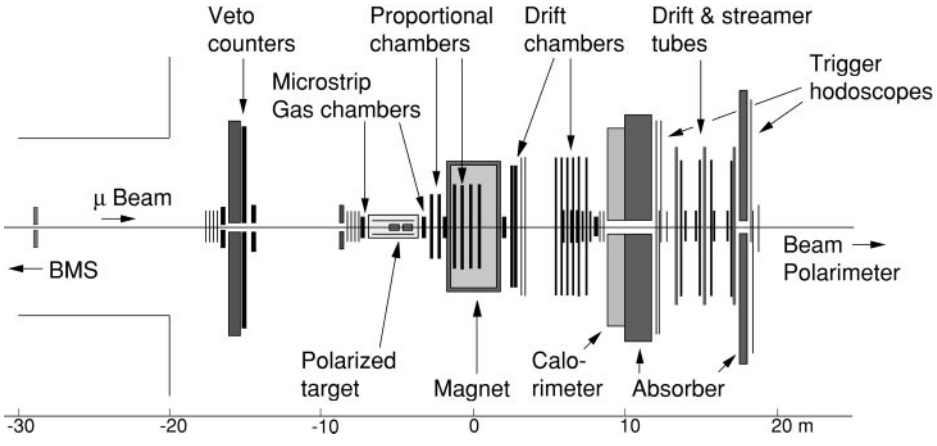

Figure 5 Schematic of the Spin Muon Collaboration spectrometer.

Annu. Rev. Nucl. Part. Sci. 1999.49:303-339. Downloaded from arjournals.annualreviews.org
by MASSACHUSETTS INSTITUTE OF TECHNOLOGY on 05/05/08. For personal use only.

storage cells with either pure hydrogen, deuterium, or helium-3 targets. The spectrometer (Figure 6) consists of a large magnet followed by a detector package. The magnet bends charged particles produced in the interactions at the target, and the detectors are used for particle identification and momentum determination. The detector package in HERMES relies on a threshold Cerenkov counter and transition radiation detector for particle identification and tracking chambers with a rear lead-glass calorimeter for momentum and energy determination. Recently,

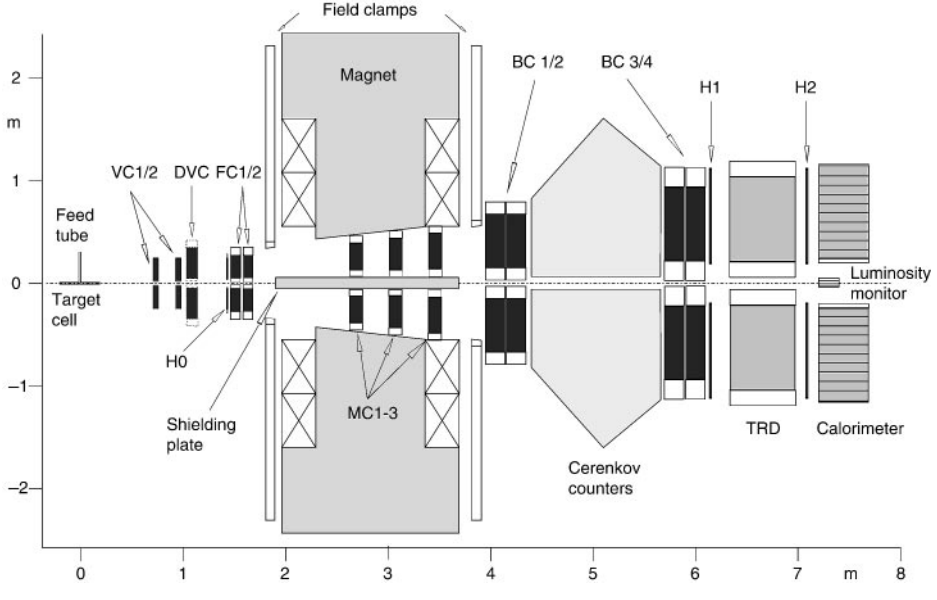

Figure 6 Schematic of the HERMES experiment installed at the DESY HERA storage ring.

a Cerenkov ring imaging detector has been installed at HERMES to tag hadrons and, in particular, kaons produced in the DIS interactions.

The beam operates in a continuous mode, so it is straightforward to tag final-state particles for studies of semi-inclusive scattering (Section 5.2). The strength of the HERMES program lies in its clean identification of the interaction and complete event reconstruction using pure polarized gas targets.

Annu. Rev. Nucl. Part. Sci. 1999.49:303-339. Downloaded from arjournals.annualreviews.org
by MASSACHUSETTS INSTITUTE OF TECHNOLOGY on 05/05/08. For personal use only.

4. RECENT RESULTS ON SPIN-DEPENDENT STRUCTURE FUNCTIONS

Whereas early determinations of the structure function g_1 relied only on measurements of the asymmetry $A_\parallel$ and had to assume $g_2 = 0$, recent experiments have also measured the transverse asymmetry $A_\perp$. They can thus determine g_1 and g_2 simultaneously from $A_\parallel$ and straightforwardly determine $A_\perp$ from the experimental asymmetries, following the formalism outlined in Section 5.2. In this analysis, the deep inelastic cross sections and cross-section asymmetries must be corrected for higher-order quantum-electrodynamic radiative effects, details of which are outside the scope of this chapter (see e.g. 40, 51).

The unpolarized structure functions F_1, or F_2 and R, are also necessary to convert the cross-section asymmetries into spin structure functions (Equations 13 and 14). This analysis relies on parameterizations (44) of recent high-precision measurements of F_2 and R made at SLAC, CERN, Fermilab, and DESY.

The experiments cover different ranges in x and Q^2 owing to their different beam energies and different coverage of scattering angles. Figure 7 shows the kinematic domains of recent measurements of g_1; the kinematic regions of the g_2 data are similar. Because QCD predicts a Q^2 dependence of the spin structure functions (Section 2.5), results on $g_1(x)$ and $g_2(x)$ from different experiments cannot be compared directly. For g_1, results from electron- and muon-scattering experiments with proton, deuteron, and neutron targets are shown in Figure 8. Figure 9 presents recent measurements of g_1^p from the HERMES experiment at DESY compared with the CERN and SLAC data. Measurements of g_2 in the E143 and E155 experiments are shown in Figure 10.

5. POLARIZED PARTON DISTRIBUTIONS AND THE SPIN STRUCTURE OF THE PROTON

5.1 Polarized Parton Distributions from a Next-to-Leading Order Quantum Chromodynamics Analysis

The QCD formalism outlined in Section 2.5 allows the determination of polarized parton distributions from the measured x and Q^2 dependence of the structure function g_1. Complete NLO analyses have been presented by the SLAC E154 (72) and SMC (73) collaborations. Their analyses are similar and both use the

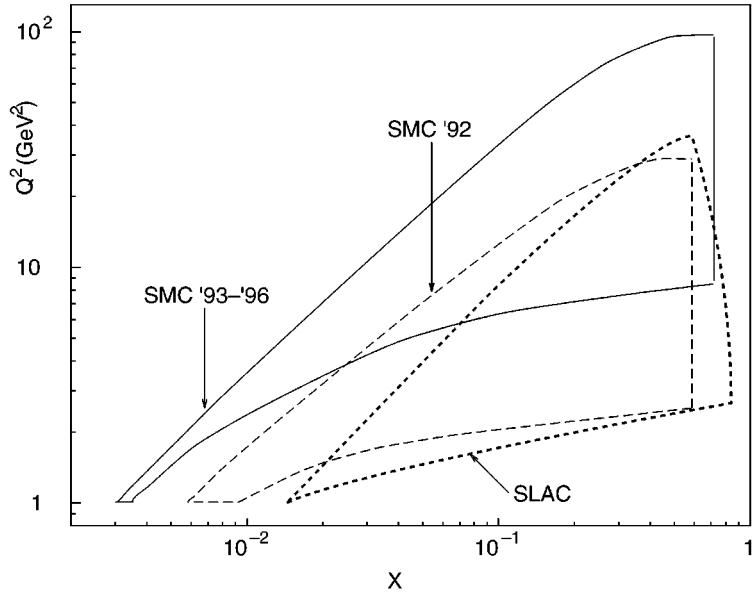

Figure 7 Kinematic domains of recent measurements of $g_1(x, Q^2)$. For the Spin Muon Collaboration, there are two different regions because different beam energies were used in 1992 (100 GeV) and in 1993–1996 (190 GeV). The SLAC curve indicates the combined domain covered by experiments E142, E143, E154, and E155. The HERMES domain is roughly similar to SLAC's but starts at $x = 0.03$.

complete set of world data available at the time of the analysis. We focus here on the more recent SMC analysis, which includes the final set of SMC proton data.[2]

The polarized singlet, nonsinglet, and gluon distributions at a fixed Q^2 are parameterized as

$$\Delta f(x, Q^2) = N(\alpha_f, \beta_f, a_f)\eta_f x^{\alpha_f}(1-x)^{\beta_f}(1+a_f x), \qquad 54.$$

where $N(\alpha, \beta, a)$ is constrained by the normalization condition

$$N(\alpha, \beta, a)\int_0^1 x^{\alpha}(1-x)^{\beta}(1+ax)\,dx = 1, \qquad 55.$$

and Δf denotes $\Delta\Sigma$ (Equation 46), Δq_{NS} (Equation 47), or ΔG. With this normalization, the parameters η_g, η_{NS}, and η_{S} are the first moments of the gluon, nonsinglet quark, and singlet quark distributions, respectively. The parton distributions are

[2]Where we show results from both analyses, it must be kept in mind that the data sets overlap considerably, and that the results are therefore strongly correlated. Small differences between the E154 and SMC results are mostly attributable to the different fitting methods.

Annu. Rev. Nucl. Part. Sci. 1999.49:303-339. Downloaded from arjournals.annualreviews.org
by MASSACHUSETTS INSTITUTE OF TECHNOLOGY on 05/05/08. For personal use only.

Annu. Rev. Nucl. Part. Sci. 1999.49:303-339. Downloaded from arjournals.annualreviews.org
by MASSACHUSETTS INSTITUTE OF TECHNOLOGY on 05/05/08. For personal use only.

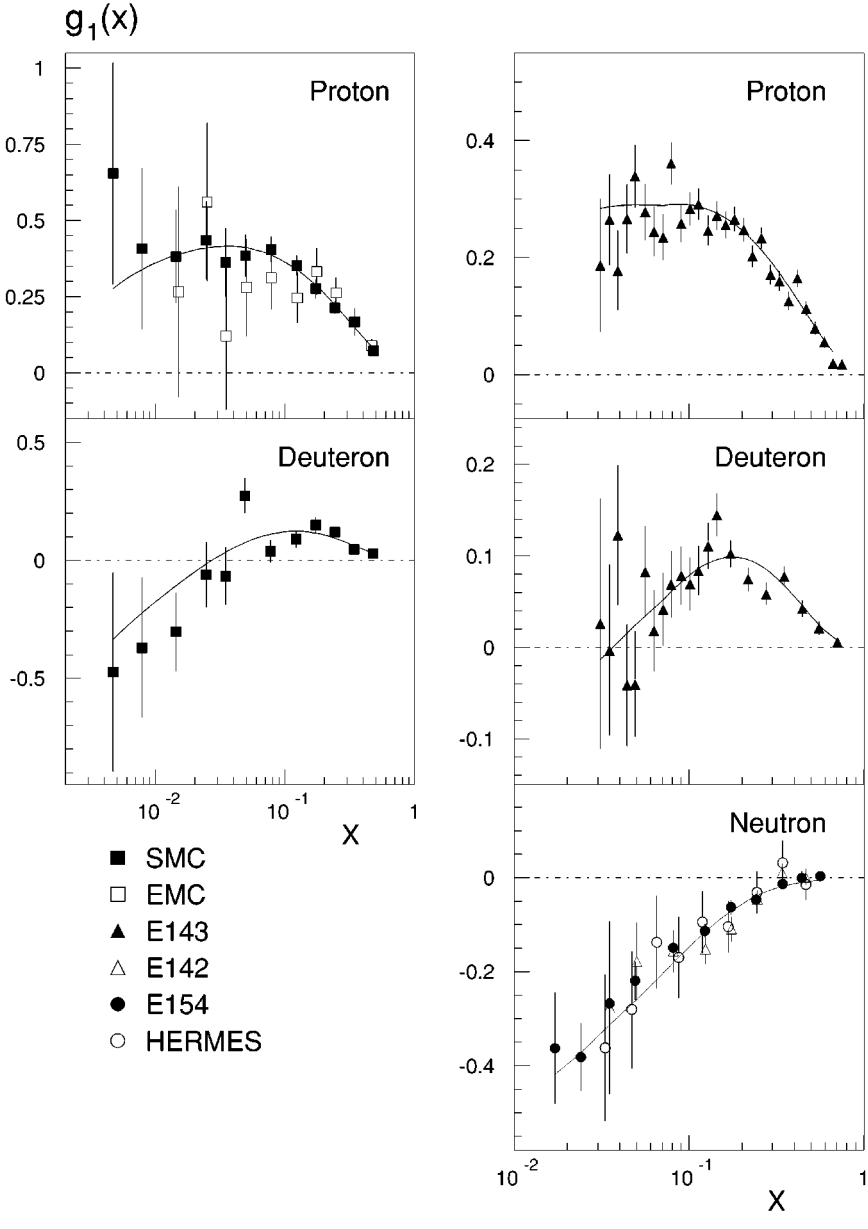

Figure 8 The structure function g_1 of the proton, the deuteron, and the neutron, as a function of x, from the CERN muon-scattering experiments (*left*) and the SLAC and DESY electron-scattering experiments (*right*). Only statistical errors are shown. Solid lines show a next-to-leading order QCD fit, discussed in Section 5.

Annu. Rev. Nucl. Part. Sci. 1999.49:303-339. Downloaded from arjournals.annualreviews.org
by MASSACHUSETTS INSTITUTE OF TECHNOLOGY on 05/05/08. For personal use only.

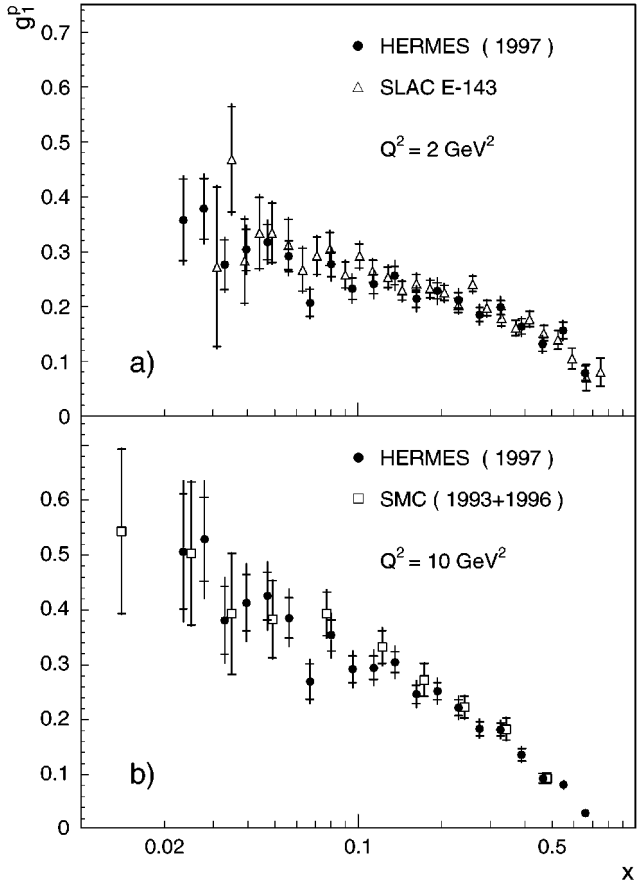

Figure 9 Recent data on the spin structure function g_1^p from the HERMES experiment at (*a*) $Q^2 = 2$ GeV^2 and (*b*) $Q^2 = 10$ GeV^2, compared with data from the SMC and SLAC E143 experiment. Inner error bars represent statistical error only; outer error bars are statistical and systematic errors combined in quadrature.

evolved to the Q^2 of the experimental data using Equations 49–51. A prediction for g_1 is computed from Equations 46–48 and fitted to the experimental data using a χ^2 minimization. For the strong coupling constant, the value $\alpha_s(M_Z^2) = 0.118 \pm 003$ from Reference 74 is used. The normalization of the nonsinglet quark densities $\eta_{\rm NS}^{\rm p,n}$ is fixed using the neutron and hyperon β-decay constants and assuming SU(3) flavor symmetry, $\eta_{\rm NS}^{\rm p,n} = \pm\frac{3}{4}\frac{g_A}{g_V} + \frac{1}{4}a_8$ with $|g_A/g_V| = F + D = 1.2601 \pm 0.0025$ (74) and $F/D = 0.575 \pm 0.016$ (75). Fits in the $\overline{\rm MS}$ and AB schemes describe the data equally well; unless stated otherwise, results shown here are obtained in the AB scheme.

Figure 11 shows the nonsinglet distributions for proton and neutron as well as the singlet and gluon distributions. Whereas the quark distributions are well

Annu. Rev. Nucl. Part. Sci. 1999.49:303-339. Downloaded from arjournals.annualreviews.org
by MASSACHUSETTS INSTITUTE OF TECHNOLOGY on 05/05/08. For personal use only.

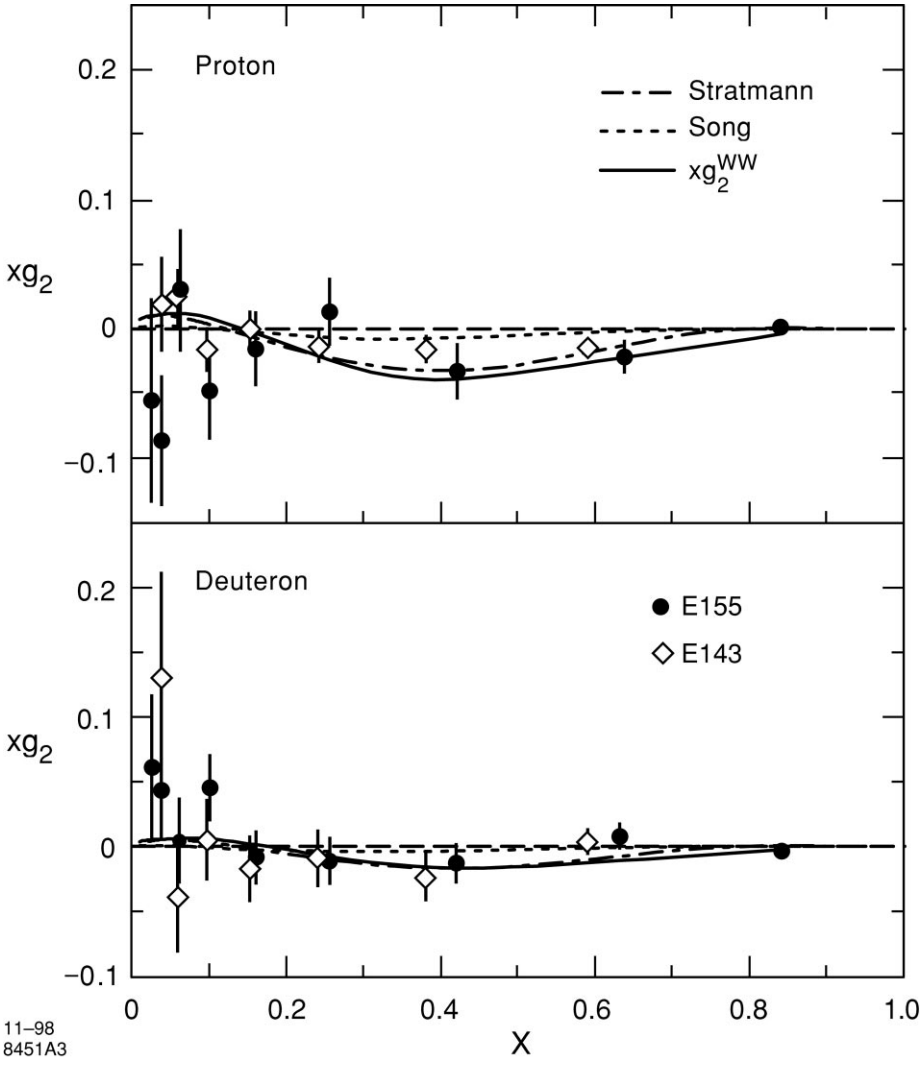

Figure 10 The spin-dependent structure function xg_2 as a function of x, measured by SLAC experiments E143 and E155, for the proton and the deuteron. Only statistical errors are shown; the systematic errors are much smaller. The solid curve shows a twist-2 calculation of g_2^{WW}. Also shown are bag model calculations at $Q^2 = 5.0$ GeV^2 by Stratmann (70) and Song (71).

Annu. Rev. Nucl. Part. Sci. 1999.49:303-339. Downloaded from arjournals.annualreviews.org
by MASSACHUSETTS INSTITUTE OF TECHNOLOGY on 05/05/08. For personal use only.

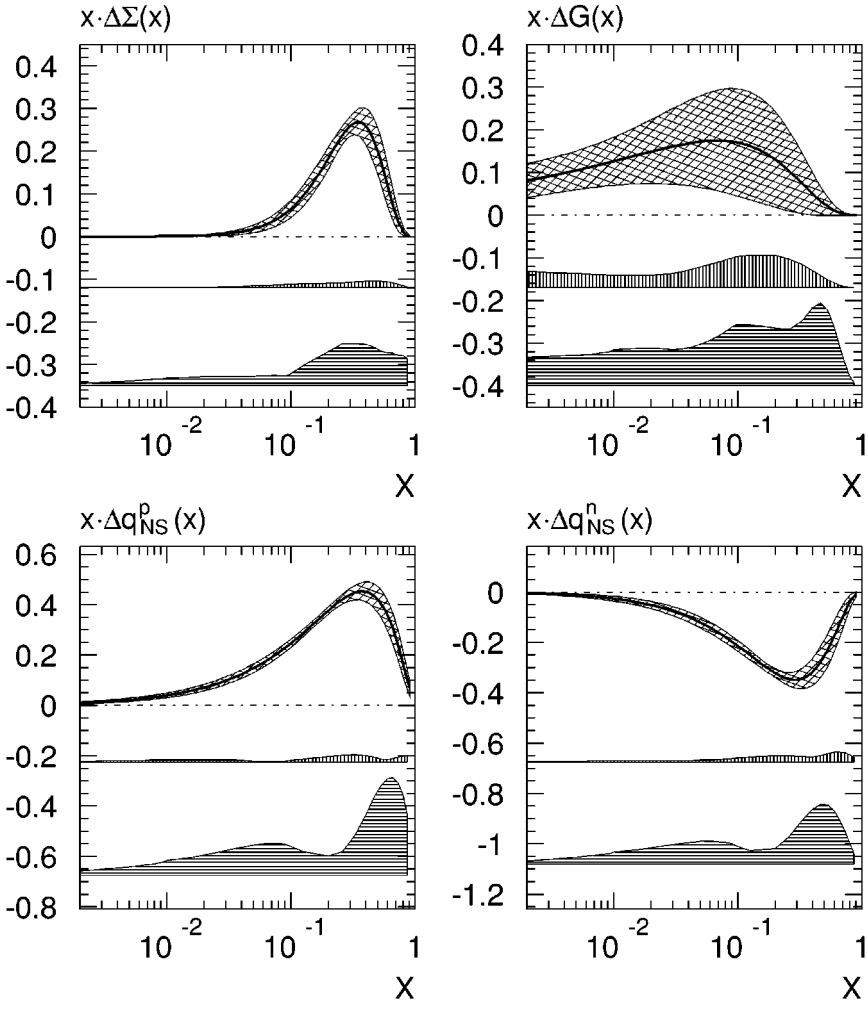

Figure 11 Polarized parton distribution functions at $Q^2 = 1\,\mathrm{GeV}^2$, obtained from a perturbative QCD analysis (73). The statistical uncertainties are indicated by the cross-hatched bands. The systematic experimental and theoretical uncertainties are indicated by the vertically and horizontally hatched bands, respectively.

determined, the gluon distribution is only marginally constrained. The structure function g_1 obtained from these fits is superimposed on the experimental data in Figure 8.

5.2 Parton Distributions From Semi-Inclusive Measurements

SMC has also made a semi-inclusive measurement of the cross-section asymmetry of final-state hadrons produced in deep inelastic muon-nucleon scattering

Annu. Rev. Nucl. Part. Sci. 1999.49:303-339. Downloaded from arjournals.annualreviews.org
by MASSACHUSETTS INSTITUTE OF TECHNOLOGY on 05/05/08. For personal use only.

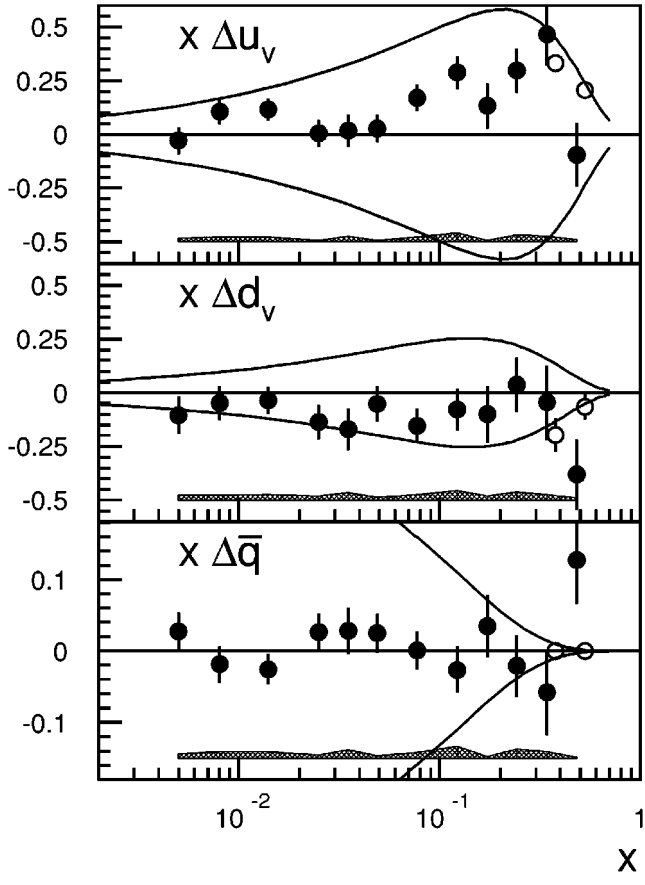

Figure 12 The polarized quark distributions $x\Delta u_v(x)$, $x\Delta d_v(x)$, and $x\Delta\bar{q}(x)$ measured by SMC, assuming $\Delta\bar{u}(x) = \Delta\bar{d}(x)$. The open circles are obtained when the sea polarization is set to zero; the solid circles are obtained without this assumption. The error bars are statistical and the shaded areas represent the systematic uncertainty. The solid lines show the limit $\pm xq(x)$ from unpolarized quark distributions at $Q^2 = 10\ \text{GeV}^2$. *Bottom*: Curves correspond to $\pm x(\bar{u}(x) + \bar{d}(x))/2$.

(76). Although the SMC spectrometer can resolve the tracks of final-state hadrons, there is no particle identification—basically, all final-state hadrons are assumed to be pions—and thus no measurement of the strange quark polarization. However, the measurement can distinguish up and down quarks by measuring the charge of the final-state hadron, and it can separate quarks from antiquarks owing to their different fragmentation functions. The sea quark polarization is evaluated assuming a flavor-SU(3)-symmetric sea.

Figure 12 shows the polarized valence quark distributions $x\Delta u_v(x)$ and $x\Delta d_v(x)$, as well as the sea quark distribution $x\Delta\bar{q}(x)$. The data exhibit a clear positive polarization of valence up quarks, a negative polarization of valence down

quarks, and a sea polarization compatible with zero. The corresponding first moments are

$$\Delta u_v = 0.77 \pm 0.10 \pm 0.08,$$

$$\Delta d_v = -0.52 \pm 0.14 \pm 0.09,$$

$$\Delta \bar{q} = 0.01 \pm 0.04 \pm 0.03.$$

The HERMES experiment is equipped for sophisticated particle identification and should soon provide much more refined data from final-state hadron asymmetries.

Annu. Rev. Nucl. Part. Sci. 1999.49:303-339. Downloaded from arjournals.annualreviews.org
by MASSACHUSETTS INSTITUTE OF TECHNOLOGY on 05/05/08. For personal use only.

5.3 Moments of Spin-Dependent Structure Functions

Sum rule tests are at the heart of testing predictions for spin-dependent structure functions. Historically, the evaluation of Γ_1 relied on a two-step approach: (*a*) evaluation of $\int g_1(x)\,dx$ at constant Q^2 in the measured x region and (*b*) phenomenological extrapolation to $x = 0$ and $x = 1$.

The extrapolation to $x = 1$ is not critical, since it is a small contribution and is safely constrained by the trivial bound $A_1 < 1$. In contrast, the small-x extrapolation is the subject of much debate and a source of substantial uncertainty. An in-depth discussion of the small-x behavior of g_1 is beyond the scope of this chapter. Most analyses have assumed for this purpose a functional form $g_1(x) \propto x^\alpha$ predicted by Regge theory, α being bound by $0 \leq \alpha \leq 0.5$ (77). Even if theoretically justified, using this form entails some arbitrariness, since Regge theory does not predict the limit in x to which the theory is actually valid.

Recent evaluations of Γ_1 rely on the NLO QCD fit discussed in Section 5.1 for the small-x and large-x extrapolations. This fit is also constrained to a Regge-type behavior at small x by the x^α term in Equation 54. Table 2 shows the results for Γ_1 for proton, deuteron, and neutron.

The same QCD analysis allows an estimate of the first moment of the polarized gluon distribution. SMC finds

$$\eta_g = \int_0^1 \Delta G(x)\,dx = 0.99^{+1.17}_{-0.31}(\text{stat.})^{+0.42}_{-0.22}(\text{syst.})^{+1.43}_{-0.45}(\text{theor.}) \qquad 56.$$

TABLE 2 $\Gamma_1^{p,d,n}$ at $Q^2 = 5\ \text{GeV}^2$ from the Spin Muon Collaboration (73) and E154 (72) next-to-leading-order QCD analysis in the AB renormalization scheme[a]

	SMC	**E154**
Proton	$0.121 \pm 0.003 \pm 0.005 \pm 0.017$	$0.114^{+0.005+0.010+0.001}_{-0.006-0.011-0.003}$
Deuteron	$0.021 \pm 0.004 \pm 0.003 \pm 0.016$	$0.029^{+0.004+0.007+0.001}_{-0.005-0.008-0.007}$
Neutron	$-0.075 \pm 0.007 \pm 0.005 \pm 0.019$	$-0.051^{+0.005+0.006+0.001}_{-0.006-0.007-0.012}$

[a]The first error is statistical, the second is systematic, and the third is an estimate of theoretical uncertainties.

at $Q^2 = 1\,\mathrm{GeV}^2$. The result for η_g is 1.7 at $Q^2 = 5\ \mathrm{GeV}^2$ and 2.0 at $Q^2 = 10\,\mathrm{GeV}^2$. The errors show that present experiments are inadequate for a conclusive measurement of η_g and direct measurements of leading-order gluon interactions will be necessary for a precise measurement of the gluon polarization (Section 7).

5.4 The Spin Structure of the Proton

For a nucleon with spin $S_z = +\frac{1}{2}$, the moments Δq of Equation 38 can be understood as normalized average z components of S_z carried by each of the quark flavors, such that $\Delta\Sigma = \Delta u + \Delta d + \Delta s$ is the total quark contribution to S_z that can be decomposed according to the helicity sum rule of Equation 1. Using the numerical results for $F + D$ and F/D quoted in Section 5.1, the Ellis-Jaffe prediction of Equation 45 is equivalent to $\Delta\Sigma = \Delta u + \Delta d \simeq 0.58$.

The total quark contribution to the proton spin, $\Delta\Sigma = a_0$, can also be obtained in a straightforward way from the QCD fit. In the $\overline{\mathrm{MS}}$ scheme, a_0 is equal to the first moment η_S of the singlet quark distribution, whereas in the AB scheme, the gluon distribution must be subtracted. Equation 52 can be rewritten as

$$a_0(Q^2) = \eta_S^{\mathrm{AB}} - n_f \frac{\alpha_s(Q^2)}{2\pi}\eta_g(Q^2). \qquad 57.$$

Figure 13 compares the results of the SMC fit for a_0 in the two renormalization schemes as a function of Q^2. As expected, the measurements are compatible for a scheme-independent quantity; they are significantly smaller than the naive QPM prediction. This observation confirms the violation of the Ellis-Jaffe sum rule first reported by the EMC (36).

It has been argued that the large discrepancy between the measured a_0 and the QPM expectation could be explained by a large gluon contribution. The small first moment of the singlet quark distribution in the AB scheme found by both experiments,

$$\mathrm{E154}: \eta_S = 0.25^{+0.07+0.05+0.05}_{-0.07-0.05-0.02}, \quad \mathrm{SMC}: \eta_S = 0.38^{+0.03+0.03+0.03}_{-0.03-0.02-0.05},$$

does not support this conjecture. The violation of the Ellis-Jaffe sum rule implies that the spin structure of the proton cannot be explained by polarized valence quarks only. However, more experiments are needed to disentangle fully the different contributions to the nucleon spin.

6. QCD TESTS

Fundamental tests of QCD are difficult to perform. The strong coupling constant is large, implying that any series expansion in powers of $\alpha_s(Q^2)$ will diverge quickly. Also, since quarks are confined in hadrons, one cannot interpret the scattering as being simply off free quarks. The difficulties associated with quark confinement complicate the interpretation of results.

Annu. Rev. Nucl. Part. Sci. 1999.49:303-339. Downloaded from arjournals.annualreviews.org
by MASSACHUSETTS INSTITUTE OF TECHNOLOGY on 05/05/08. For personal use only.

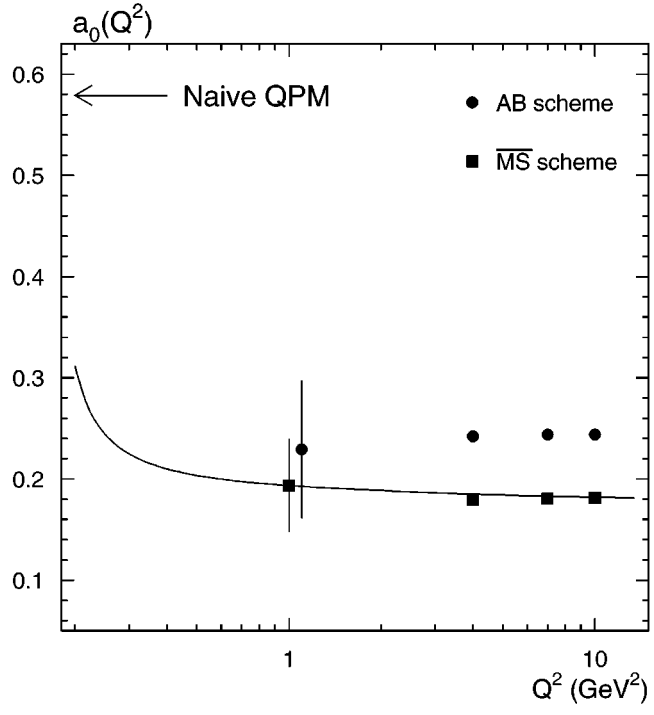

Figure 13 The total quark contribution to the proton spin obtained by SMC in the $\overline{\text{MS}}$ and AB renormalization schemes, as a function of Q^2. Statistical errors are shown only for the data points at $Q^2 = 1\,\text{GeV}^2$; the error bars for the other data points are similar. The solid line shows the predicted Q^2 evolution of a_0 in the $\overline{\text{MS}}$ scheme. Also shown is the naive quark-parton–model prediction for $\Delta s = 0$.

The behavior of the nucleon spin structure as predicted by the Bjorken sum rule, discussed in Section 2.3, does provide one such fundamental test of QCD. Although, ideally, an infinite-momentum beam would be necessary to test the Bjorken sum rule (valid at infinite Q^2), it is possible to study the sum rule at finite energies by taking into account the perturbative QCD corrections. If perturbative QCD is a valid description at finite Q^2, it should result in the same value of $\alpha_s(Q^2)$ as that provided by other experimental processes. In addition, like scaling violations in the unpolarized structure functions, scaling violations in the polarized structure functions are expected to yield a reasonably complete picture of the nucleon structure. The sum rules, parton distributions, and structure function evolutions, both unpolarized and polarized, are all highly correlated.

6.1 Tests of the Bjorken Sum Rule

The Bjorken sum rule gives a relationship between the proton and neutron integrals, $\int g_1^p(x)\,dx$ and $\int g_1^n(x)\,dx$, compared with the ratio of the axial-vector to vector

Annu. Rev. Nucl. Part. Sci. 1999.49:303-339. Downloaded from arjournals.annualreviews.org
by MASSACHUSETTS INSTITUTE OF TECHNOLOGY on 05/05/08. For personal use only.

Annu. Rev. Nucl. Part. Sci. 1999.49:303-339. Downloaded from arjournals.annualreviews.org
by MASSACHUSETTS INSTITUTE OF TECHNOLOGY on 05/05/08. For personal use only.

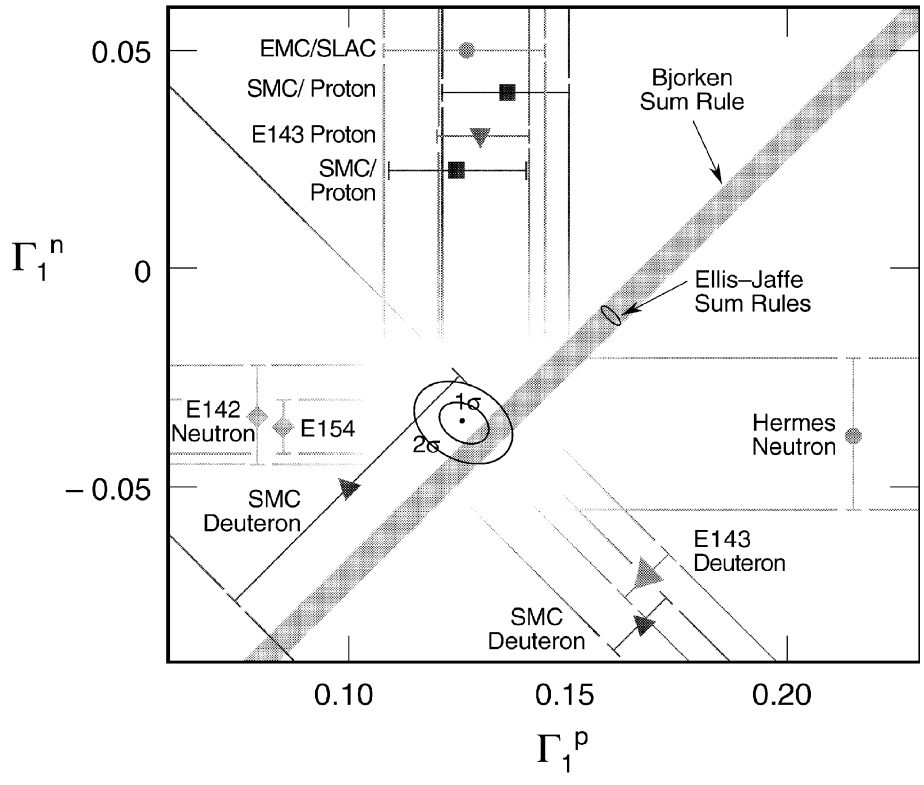

Figure 14 Measurements of the first moments Γ_1 of the spin-dependent structure function g_1 in the $\Gamma_1^p - \Gamma_1^n$ plane, from experiments at CERN, SLAC, and DESY. The results are compared with the Bjorken (line) and Ellis-Jaffe (point) sum rule predictions.

weak coupling constants, g_A/g_V. At infinite momentum transfer, the difference between the proton and neutron integrals is exactly $\frac{1}{6}g_A/g_V$. At lower Q^2, perturbative QCD corrections must be applied to the Bjorken sum rule formula. Typically, when testing the Bjorken sum rule, one evolves the spin structure function data to a fixed value of Q^2 for each value of x, using the NLO QCD formalism. One then integrates over the full x range to evaluate the proton and neutron integrals.

Each of the experimental programs resulted in a determination of the proton and neutron integrals. Figure 14 shows the neutron integral Γ_1^n plotted against the proton integral Γ_1^p. There is good agreement between all of the proton and neutron measurements and, interestingly, the EMC result for the proton remains competitive. There is also good agreement between the experiments and the Bjorken sum rule prediction, but a substantial disagreement exists between the measurements and the Ellis-Jaffe sum rule prediction. Table 3 presents the published results of the Bjorken sum rule test performed by the SMC and E154 collaborations. At the level of approximately 10%, the Bjorken sum rule is tested and confirmed.

TABLE 3 Tests of the Bjorken sum rule from the SMC (73) and E154 (72) experiments[a]

	Q^2	$\Gamma_1^p - \Gamma_1^n$	Bjorken sum rule[b]
SMC	5 GeV^2	$0.181^{+0.012+0.018+0.015}_{-0.011-0.018-0.006}$	0.181 ± 0.003
E154	5 GeV^2	$0.171 \pm 0.005 \pm 0.010 \pm 0.006$	0.181 ± 0.003

[a]The first uncertainty is statistical, the second systematic, and the third theoretical.

[b]Bjorken sum rule prediction evaluated up to order α_s^2 (11).

Annu. Rev. Nucl. Part. Sci. 1999.49:303-339. Downloaded from arjournals.annualreviews.org
by MASSACHUSETTS INSTITUTE OF TECHNOLOGY on 05/05/08. For personal use only.

The Bjorken sum rule test is limited by systematic uncertainties coming primarily from the beam and target polarization uncertainties, as well as by theoretical uncertainties arising from the limited beam energies.

Significant improvement on Bjorken sum rule testing would require a substantially higher-energy experiment. At higher energies, the theoretical uncertainties coming from the low x extrapolation and from the perturbative QCD corrections are reduced. Such an experiment would also require meticulous control over the beam and target polarizations, at the level of ~1% or better. No such program is currently in sight.

6.2 Determination of the Strong Coupling Constant α_s

Equivalent to the analysis in the last section, one can accept the validity of the Bjorken sum rule and use it along with the experimental results to extract a value of the strong coupling constant $\alpha_s(Q^2)$. Perturbative QCD provides corrections to the Bjorken sum rule so that the relationship has a meaning when Q^2 is finite.

Armed with the measured proton and neutron spin structure function integrals, one can simply solve for the strong coupling constant α_s in Equation 34. Using the first measurements of the proton and neutron integrals, Ellis & Karliner found $\alpha_s(M_Z^2) = 0.122 \pm 0.006$ (78) evaluated at the Q^2 of the mass of the Z boson. In a recent analysis, SMC finds $\alpha_s(M_Z^2) = 0.121 \pm 0.002 \pm 0.006$, where the first error is statistical and the second combines systematical and theoretical uncertainties (73). This is in good agreement with the values from other experiments. This determination of $\alpha_s(M_Z^2)$ is approximately a factor of two less precise than the most competitive determinations of $\alpha_s(M_Z^2)$.

6.3 Scaling Violations of Spin Structure Functions

In the naive QPM, the cross section for scattering off partons does not depend on the four-momentum of the virtual photon. However, in the framework of QCD, gluon emission occurs, and as a result, the cross section will vary for a fixed value of x as Q^2 is varied. The rise in the unpolarized structure function F_2 at low x and the decrease of F_2 at high x as Q^2 increases are evidence of the effect of gluons. The fact that F_2 depends on Q^2 is called "scaling violations." The DGLAP evolution equations provide a prediction for the change in the structure function with Q^2. Section 2.5 describes the NLO QCD formalism of these equations.

Annu. Rev. Nucl. Part. Sci. 1999.49:303-339. Downloaded from arjournals.annualreviews.org
by MASSACHUSETTS INSTITUTE OF TECHNOLOGY on 05/05/08. For personal use only.

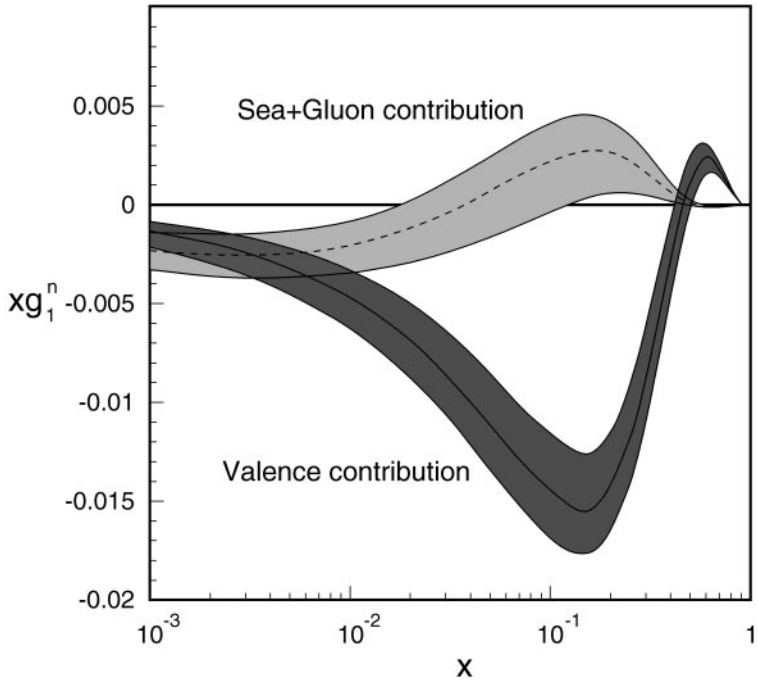

Figure 15 Sea, gluon, and valence contributions to the spin structure function g_1^n from a next-to-leading-order fit to the world data by the E154 collaboration.

The power of the NLO equations is that they appear to provide a reasonably complete and consistent picture of the polarized parton distributions in the nucleon. Figure 15 gives the results from a NLO analysis separating the valence and gluon contributions and depicting their contribution to the neutron spin structure function, g_1^n. At very low x, the sea quark and gluon contributions eventually dominate. If the gluon contribution is neglected, the fits become mildly worse, and, more important, the low-x behavior of the neutron spin structure function starts to become divergent. In short, the existence of a reasonably complete picture of the nucleon spin structure in terms of polarized quark and gluon distributions in the context of perturbative QCD represents one fundamental test of QCD. This situation is reminiscent of the early years of the proton structure studies (79), when the scaling violations for the unpolarized structure functions were discovered and unraveled.

7. FUTURE DETERMINATIONS OF THE GLUON SPIN DISTRIBUTIONS

The enormous data sample provided by the polarized deep inelastic fixed-target scattering experiments has allowed a reasonably precise determination of the polarized parton distributions. In the near future, additional experimental information

is unlikely to have any significant impact on the determination of the quark contribution to the proton spin (besides the semi-inclusive DIS scattering program begun at HERMES). Extracting the gluon contribution to the proton spin is another story. Several groups are gearing up to study the polarized gluon contribution.

Scaling violations of the nucleon spin structure functions, g_1^p and g_1^n, have already given a first glimpse of the gluon spin contribution to the nucleon spin. Figure 11 indicates at the level of approximately two standard deviations a positive ΔG contribution. However, major improvements in determining ΔG are not expected to come from inclusive polarized deep inelastic scattering any time soon.

The main lines of attack for measuring ΔG will come from exclusive reactions in which one measures an outgoing final state particle resulting from spin-dependent gluon interactions. These measurements of ΔG over some kinematic range in x and Q^2 are being tried both at polarized collider experiments and at polarized fixed-target experiments. Figure 16 presents models for ΔG (until now essentially

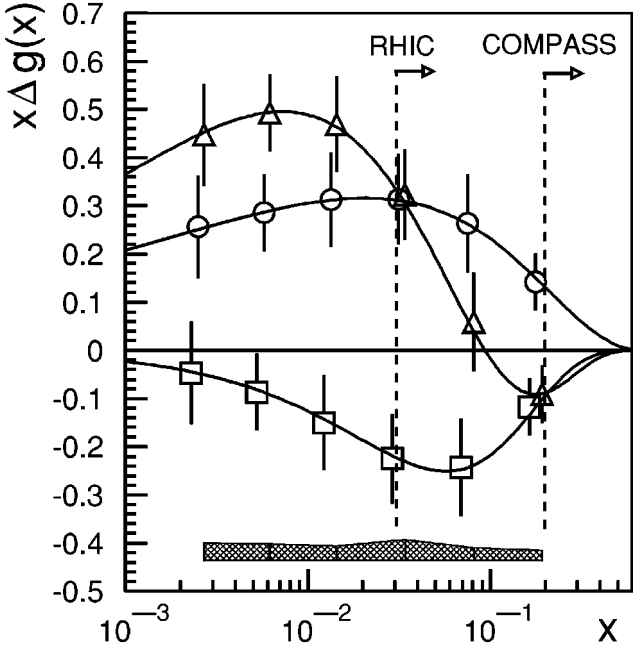

Figure 16 The polarized gluon distribution $x\Delta G$ in different models. The curve with circles superimposed shows $x\Delta G$ from a next-to-leading-order QCD fit to the SMC g_1 data. Triangles show gluon set C in the model of Gehrmann & Stirling (28). Squares show an instanton-induced gluon polarization proposed by Kochelev et al (80). Error bars indicate the statistical sensitivity of a measurement with dijet events with polarized beams of HERA for an integrated luminosity of 500 pb^{-1}; the corresponding systematic uncertainty is indicated by the band. Also shown are the x ranges accessible to experiments at RHIC and COMPASS (from Reference 81).

Annu. Rev. Nucl. Part. Sci. 1999.49:303-339. Downloaded from arjournals.annualreviews.org
by MASSACHUSETTS INSTITUTE OF TECHNOLOGY on 05/05/08. For personal use only.

untested) and the different x ranges covered by the experimental efforts discussed in the subsequent sections. As expected, the lower-energy fixed-target experiments are aimed at extracting ΔG at relatively high values of x, whereas the collider experiments will search for ΔG at low x values.

7.1 Experiments with Polarized Proton-Proton Colliders

Although theoretically challenging, scattering of polarized protons on polarized protons at high energies represents one method to study polarized quark-quark interactions. In particular, by tagging a hard outgoing photon in the interaction, it is possible to access information on the polarized gluon distribution. Such a study requires information on the fragmentation processes and a means of contending with background processes, such as those coming from the production and subsequent decay of neutral pions.

An experimental program has been approved at the RHIC collider at Brookhaven National Laboratory. Here, beams of polarized protons colliding at 250 GeV will be studied in the STAR and PHOENIX detectors. Although the full program to obtain the gluon spin distribution from polarized proton-proton collisions will require a careful study of complicated background processes, the polarized RHIC program does offer one of the first high-energy efforts to determine ΔG at low x, where the gluon interactions are expected to dominate. These experiments aim to measure ΔG to a precision of ± 0.1 over the x range from 0.02 to 0.2. These measurements will complement the fixed-target studies.

7.2 Experiments with Polarized-Electron–Polarized-Proton Colliders

Probably the most exciting opportunity to study the polarized gluon distribution would come from an extremely high-energy polarized-electron–polarized-proton collider. The HERA collider at DESY with the ZEUS and H1 experiments would offer such an opportunity. At DESY, 30-GeV electrons will collide with nearly 1-TeV protons to study the spin structure functions at extremely low x values (near 10^{-4} to 10^{-5}) as well as final-state jet production resulting from polarized gluon interactions. Initial studies would focus on measurements of scaling violations in the polarized proton structure function down to very low x values, significantly pinning down the gluon behavior at low x. A similar study on the unpolarized gluon distribution has already been performed at DESY. Figure 17 presents results on the gluon distribution $g(x)$ from an analysis by the H1 collaboration (82). Jet production from various processes such as charm production would give an independent measure of ΔG in a kinematic range where gluon contributions are expected to be large. First simulations of ΔG studies at DESY predict a precision on ΔG of ± 0.1 over the largest kinematic range, from x of 0.001 to 0.2.

Although this would be the cleanest approach to finding ΔG, this measurement requires the implementation of a polarized proton beam, which is not currently available at DESY. The project to upgrade the high-energy proton beam at HERA

Annu. Rev. Nucl. Part. Sci. 1999.49:303-339. Downloaded from arjournals.annualreviews.org
by MASSACHUSETTS INSTITUTE OF TECHNOLOGY on 05/05/08. For personal use only.

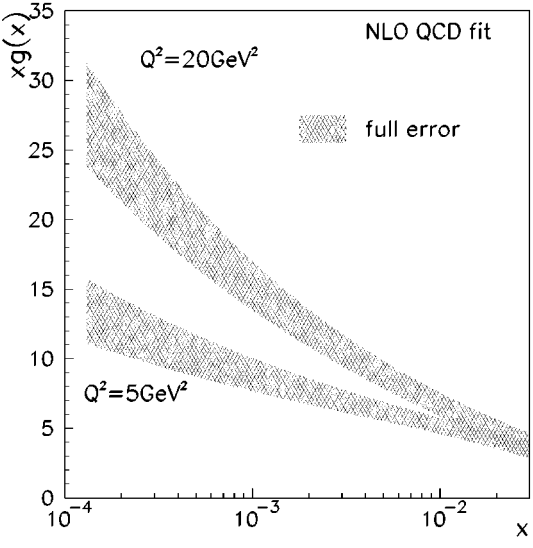

Figure 17 Unpolarized gluon distribution of the proton from the H1 collider experiment at DESY.

to include polarized proton operation is presently under review. If approved, the program would begin in approximately five years.

7.3 Future Experiments on Polarized Lepton Scattering on Fixed Polarized Targets

Two new fixed-target programs involving polarized lepton-nucleon scattering are aimed at determinations of ΔG at high x. One is the HERMES experiment, which is being upgraded to maximize the detection of final-state muons produced in electron interactions, and the other is the COMPASS experiment at CERN, which is a dedicated high-energy muon-scattering experiment. Both will use polarized lepton scattering off polarized targets and will collect data on ΔG soon after the year 2000. The process by which these experiments will hunt for ΔG is to detect open charm or J/Ψ production coming from DIS interactions. These processes depend heavily on gluon emission from the nucleon. Both experiments aim to determine ΔG to a precision of approximately ± 0.1 to ± 0.3 over the range of x from 0.1 to 0.4. The advantage of the fixed-target experiment is that it can measure ΔG at higher x and will typically collect data earlier than the technically more challenging collider experiments.

8. SUMMARY AND CONCLUSIONS

Polarized deep inelastic scattering remains one of the cleanest tests for studying the internal spin structure of the proton and neutron. Pioneering experiments at SLAC, scattering polarized electrons off polarized protons, helped establish the quark

Annu. Rev. Nucl. Part. Sci. 1999.49:303-339. Downloaded from arjournals.annualreviews.org
by MASSACHUSETTS INSTITUTE OF TECHNOLOGY on 05/05/08. For personal use only.

Annu. Rev. Nucl. Part. Sci. 1999.49:303-339. Downloaded from arjournals.annualreviews.org
by MASSACHUSETTS INSTITUTE OF TECHNOLOGY on 05/05/08. For personal use only.

structure of the proton with the observation of large spin-dependent asymmetries. An exciting follow-up experiment (CERN EMC) at higher energies uncovered a violation of a QPM sum rule, implying that the quarks accounted for only a small fraction of the proton spin—and giving birth to the proton-spin crisis. Today, a large sample of data from polarized fixed-target experiments at SLAC, CERN, and DESY have resulted in a substantial perturbative-QCD analysis of the nucleon spin structure. A few of the results of this work are summarized.

The Bjorken sum rule derived prior to the existence of QCD depending on the quark charge assignments, isospin symmetry and current algebra has now been tested and confirmed at the 10% level. From this study, a value of $\alpha_s(M_Z^2) = 0.122 \pm 0.006$ has been obtained.

The total quark contribution to the nucleon spin is measured to be approximately 30%, with the remainder presumably coming from gluon and orbital angular momentum contributions. Within this context, the up and down quark contributions to the proton spin are found to be $\sim 70\%$ and $\sim -40\%$, respectively.

Semi-inclusive scattering, which tags outgoing hadrons in deep inelastic scattering interactions, appears to confirm the up and down quark contributions to the spin, although at present the uncertainties are still rather large.

The polarized gluon contribution, which is largely responsible for scaling violations, appears to be positive, although quite poorly determined at this time. A major motivation for future high-energy polarized scattering experiments is to obtain more information on the polarized gluon contributions to the nucleon spin.

The study of the spin structure of the proton and neutron continues with active programs around the world. Further studies of semi-inclusive scattering with tagged kaons will give the first direct measurement of the strange sea contribution to the proton spin. Collider projects involving polarized-proton–polarized-proton scattering at Brookhaven or polarized-electron–polarized-proton scattering at DESY will undoubtedly provide significant information on the gluon piece of the nucleon spin puzzle. The high-energy experiments should be able to test the gluon contribution at low x, where the gluons are expected to contribute substantially.

For 30 years, studies of the internal spin structure of the proton have advanced steadily using the technology of polarized beams and polarized targets. The demand for higher-energy experiments to access the deepest regions inside the proton and to extract the theoretically cleanest results continues. We expect more puzzles, more crises, and more excitement as the future unfolds.

Visit the Annual Reviews home page at http://www.AnnualReviews.org

LITERATURE CITED

1. Ji X. *Phys. Rev. Lett.* 78:610 (1997)
2. Halzen F, Martin AD. *Quarks and Leptons.* New York: Wiley & Sons (1984); Roberts RG. *Structure of the Proton: Deep Inelastic Scattering.* Cambridge, UK: Cambridge Univ. Press (1990)
3. Jaffe RL. *Comments Nucl. Part. Phys.* 19: 239 (1990)

Annu. Rev. Nucl. Part. Sci. 1999.49:303-339. Downloaded from arjournals.annualreviews.org
by MASSACHUSETTS INSTITUTE OF TECHNOLOGY on 05/05/08. For personal use only.

4. Hoodbhoy P, et al. *Nucl. Phys.* B312:571 (1989); Rodriguez MA. *Measurement of the spin-dependent structure function g_1 of the nucleon through polarized deep inelastic muon-nucleon scattering.* PhD thesis. Univ. Santiago di Compostela (1994)
5. Doncel MG, de Rafael E. *Nuovo Cim.* 4A:363 (1971); Gnädig P, Niedermayer F. *Nucl. Phys.* B55:612 (1973)
6. Wandzura S, Wilczek F. *Phys. Lett.* B72: 195 (1977)
7. Bjorken JD, *Phys. Rev.* 148:1467 (1966); *Phys. Rev. D* 1:465 (1970); *Phys. Rev. D* 1:1376 (1970)
8. Kodaira J, et al. *Phys. Rev. D* 20:627 (1979); Kodaira J, et al. *Nucl. Phys.* B159: 99 (1979)
9. Larin SA. *Phys. Lett.* B334:192 (1994)
10. Kodaira J. *Nucl. Phys.* B165:129 (1980)
11. Larin SA, Tkachev FV, Vermaseren JAM. *Phys. Rev. Lett.* 66:862 (1991); Larin SA, Vermaseren JAM. *Phys. Lett.* B259:345 (1991); Larin SA. CERN-TH-7208/94. hep-ph/9403383 (1994)
12. Kataev AL, Starshenko V. CERN-TH-7198/94. hep-ph/9405294 (1994)
13. Ellis J, Jaffe RL. *Phys. Rev. D* 9:1444 (1974); *Phys. Rev. D* 10:1669 (1974)
14. Kataev AL. CERN-TH-7333/94 (1994)
15. Ellis J, Karliner M. *Phys. Lett.* B313:131 (1993); *Phys. Lett.* B341:397 (1995)
16. Shuryak EV, Vainshtein AI. *Nucl. Phys.* B201:141 (1982)
17. Balitsky II, Braun VM, Kolesnichenko AV. *Phys. Lett.* B242:245 (1990); Erratum, B318:648 (1993)
18. Close FE, Roberts RG. *Phys. Lett.* B316: 165 (1993)
19. Ji X, Unrau P. MIT-CTP-2232. hep-ph/ 9308263 (1993)
20. Burkert VD, Ioffe BL. CEBAF-PR-92-018 (1992)
21. Ehrnsperger B, Schäfer A, Mankiewicz L. *Phys. Lett.* B323:439 (1994)
22. Ross GG, Roberts RG. *Phys. Lett.* B322: 425 (1994)
23. Stein E, et al. UFTP 366/1994. hep-ph/ 9409212 (1994)
24. Altarelli G. *Phys. Rep.* 81:1 (1982)
25. Dokshitzer YuL. *Sov. Phys. JETP* 46:461 (1977)
26. Altarelli G, Parisi G. *Nucl. Phys.* B126:298 (1977)
27. Gribov VN, Lipatov LN. *Sov. J. Nucl. Phys.* 15:438,675 (1972)
28. Gehrmann T, Stirling WJ. *Z. Phys. C* 65:461 (1995); *Phys. Rev.* D 53:6100 (1996)
29. t'Hooft G, Veltman M. *Nucl. Phys.* B44: 189 (1972)
30. Ball RD, Forte S, Ridolfi G. *Phys. Lett.* B378:255 (1996)
31. Altarelli G, Ross GG. *Phys. Lett.* B212:391 (1988); Efremov AV, Teryaev OV. JINR Rep. No. E2-88-287, Dubna 1988; Carlitz RD, Collins JC, Mueller AH. *Phys. Lett.* B214:229 (1988)
32. Mertig R, van Neerven WL. *Z. Phys. C* 70: 637 (1996)
33. Vogelsang W. *Phys. Rev. D* 54:2023 (1996)
34. Alguard MJ, et al (SLAC E80 Collaboration). *Phys. Rev. Lett.* 37:1261 (1976); *Phys. Rev. Lett.* 41:70 (1978)
35. Baum G, et al (SLAC E130 Collaboration). *Phys. Rev. Lett.* 51:1135 (1983); Baum G et al. *Phys. Rev. Lett.* 45:2000 (1980)
36. Ashman J, et al (EMC). *Phys. Lett.* B206:364 (1988); Ashman J et al. *Nucl. Phys.* B328:1 (1989)
37. Adeva B, et al (SMC). *Phys. Lett.* B302:533 (1993)
38. Adams D, et al (SMC). *Phys. Lett.* B329:399 (1994); Erratum, B339:332 (1994)
39. Adams D, et al (SMC). *Phys. Lett.* B336: 125 (1994)
40. Adeva B, et al (SMC). *Phys. Rev. D* 56: 5330 (1997)
41. Adams D, et al (SMC). *Phys. Lett.* B357: 248 (1995)
42. Adams D, et al (SMC). *Phys. Lett.* B396: 338 (1997)

Annu. Rev. Nucl. Part. Sci. 1999.49:303-339. Downloaded from arjournals.annualreviews.org
by MASSACHUSETTS INSTITUTE OF TECHNOLOGY on 05/05/08. For personal use only.

43. Adeva B, et al (SMC). *Phys. Lett.* B412:414 (1997)
44. Adeva B, et al (SMC). *Phys. Rev. D* 58: 112001 (1998)
45. Anthony PL, et al (E142 Collaboration). *Phys. Rev. Lett.* 71:959 (1993)
46. Anthony PL, et al (E142 Collaboration). *Phys. Rev. D* 54:6620 (1996)
47. Abe K, et al (E143 Collaboration). *Phys. Rev. Lett.* 74:346 (1995)
48. Abe K, et al (E143 Collaboration). *Phys. Rev. Lett.* 75:25 (1995)
49. Abe K, et al (E143 Collaboration). *Phys. Rev. Lett.* 76:587 (1996)
50. Abe K, et al (E143 Collaboration). *Phys. Rev. Lett.* 78:815 (1997)
51. Abe K, et al (E143 Collaboration). *Phys. Rev. D* 58:112003 (1998)
52. Abe K, et al (E154 Collaboration). *Phys. Rev. Lett.* 79:26 (1997)
53. Abe K, et al (E154 Collaboration). *Phys. Lett.* B404:377 (1997)
54. Ackerstaff K, et al (HERMES Collaboration). *Phys. Lett.* B404:383 (1997)
55. Airapetian A, et al (HERMES Collaboration). *Phys. Lett.* B442:484 (1998)
56. Hughes VW, Kuti J. *Annu. Rev. Nucl. Part. Sci.* 33:611 (1983)
57. Kokkedee JJ. *The Quark Model.* New York: Benjamin (1969)
58. Prescott CV, et al. *Phys. Lett.* B77:347 (1978); *Phys. Lett.* B84:524 (1979)
59. Souder PA, et al. *Phys. Rev. Lett.* 65:694 (1990)
60. Prepost R, Maruyama T. *Annu. Rev. Nucl. Part. Sci.* 45:41 (1995)
61. Doble N, et al. *Nucl. Instrum. Methods Phys. Res. A* 343:351 (1994)
62. Lederman LM, Tannenbaum MJ. In *Advances in Particle Physics,* Vol. I, p. 11. New York: NY Acad. Sci. (1968); Navarria FL. *Rivista Nuovo Cim.* 6:1 (1983)
63. Brown SC, et al. *Proc. 4th Int. Workshop on Polarised Target Materials and Techniques,* Bonn 1984, ed. W Meyer.
64. Allkofer OC, et al (EMC). *Nucl. Instrum. Methods* 179:445 (1981)
65. Adeva B, et al (SMC). *Nucl. Instrum. Methods Phys. Res. A* 343:363 (1994)
66. Adeva B, et al (SMC). CERN-EP/99-090
67. Adeva B, et al (SMC). CERN-EP/99-31
68. Ackerstaff K, et al (HERMES Collaboration). *Nucl. Instrum. Methods A* 417:230 (1998)
69. Sokolov AA, Ternov IM. *Sov. Phys. Doklady* 8:1203 (1964)
70. Stratmann M. *Z. Phys. C* 60:763 (1993)
71. Song X. *Phys. Rev. D* 54:1955 (1996)
72. Abe K, et al (E154 Collaboration). *Phys. Lett.* B405:180 (1997)
73. Adeva B, et al (SMC). *Phys. Rev. D* 58: 112002 (1998)
74. Particle Data Group, Barnett RM, et al. *Phys. Rev. D* 54:1 (1996)
75. Close FE, Roberts RG. *Phys. Lett.* B316: 165 (1993)
76. Adeva B, et al (SMC). *Phys. Lett.* B420:180 (1998)
77. Heimann RL. *Nucl. Phys.* B64:429 (1973); Ellis J, Karliner M. *Phys. Lett.* B213:73 (1988)
78. Ellis J, Karliner M. *Phys. Lett.* B341:397 (1995)
79. Mishra S, Sciulli F. *Annu. Rev. Nucl. Part. Sci.* 39:259 (1989)
80. Kochelev NI, et al. hep-ph/9711226 (1997)
81. De Roeck A, et al. DESY 97-249. hep-ph/9801300 (1998)
82. Aid S, et al (H1 Collaboration). *Nucl. Phys.* B470:3 (1996)

Annual Review of Nuclear and Particle Science
Volume 49, 1999

CONTENTS

Annu. Rev. Nucl. Part. Sci. 1999.49:303-339. Downloaded from arjournals.annualreviews.org
by MASSACHUSETTS INSTITUTE OF TECHNOLOGY on 05/05/08. For personal use only.